5-2018

Properties of Epitaxial Sr0.5Ba0.5MnO3 Films from First-Principles

Temuujin Bayaraa
University of Arkansas, Fayetteville

Properties of Epitaxial $Sr_{0.5}Ba_{0.5}MnO_3$ Films from First-Principles

A thesis submitted in partial fulfillment
of the requirements for the degree of
Master of Science in Physics

by

Temuujin Bayaraa
National University of Mongolia
Bachelor of Science in Nuclear Technology, 2012

May 2018
University of Arkansas

This thesis is approved for recommendation to the Graduate Council.

Laurent Bellaiche, Ph.D.
Thesis Director

Sergey Prosandeev, Ph.D.
Committee Member

Hugh Churchill, Ph.D.
Committee Member

Abstract

Magnetoelectric multiferroics, that possess coupled magnetic and electric degrees of freedom, have been receiving ever renewed attention for more than 15 years since they hold promise for the design of novel devices exploiting their cross-coupling.

In this thesis, we present the results of first-principles studies on physical properties of multiferroic $Sr_{0.5}Ba_{0.5}MnO_3$ films under epitaxial compressive and tensile strains, and chemical ordering. We start by reviewing multiferroic materials, a magnetoelectric coupling mechanism and then we give a brief introduction to the first-principles computational methods that are involved in this study.

Here, we report that $Sr_{0.5}Ba_{0.5}MnO_3$ (SBM) films under compressive strain become strongly polar ferromagnet with a large axial ratio and with its properties being controllable by an external knob such as a magnetic field or strain. Furthermore, we investigated SBM films subject to epitaxial strain continuously varying from relatively large compressive to relatively large tensile values and surprisingly found, in addition to previously documented tetragonal and orthorhombic states, a novel phase that has been overlooked in the recent intensive literature on SBM systems. This latter phase adopts a monoclinic symmetry and allows the polarization to rotate continuously between out-of-plane and in-plane directions, which results in giant physical responses such as large piezoelectricity. Moreover, the strain boundaries separating tetragonal, monoclinic and orthorhombic phases are predicted to be rather sensitive to the magnetic ordering (e.g., they significantly differ between G-type antiferromagnetic and ferromagnetic spin arrangements), which therefore hints at the exciting possibility of inducing structural phase transitions (e.g., from tetragonal to monoclinic or orthorhombic to monoclinic) by applying a magnetic field. Such latter effect constitutes another novel and giant magnetoelectric effect.

Acknowledgement

I still remember myself been an enthusiastic nomad who was eager to start his study at the University of Arkansas. Last two years, I have come to encounter a lot of obstacles which I could not have overcome without the help of wonderful people around me, specially my lovely wife and son. Here, I would like to take this opportunity to thank those who helped me and stood beside me throughout the years.

First, I would like to express my deepest gratitude to my family and my parents for their overflowing support and love.

Second and foremost, I would like to express my sincere gratitude to my advisor Professor Laurent Bellaiche for his teachings, guidance, and patience. This work would not have been possible without the help of Dr. Yurong Yang, Dr. Hongjian Zhao and Dr. Jorge Íñiguez and I would like to express my gratitude for their teachings, advice and time.

Further thanks to my friends and fellow graduate students for their help and friendships. And I would like to express my gratitude to Dr. Bronson Stilwell and Evelyn Stilwell for their welcoming hospitality and kindness.

Finally, I would like to express my gratitude to the Fulbright Mongolian Government Scholarship for this wonderful opportunity to study, experience new culture, meet new wonderful people and achieving new horizon.

Contents

List of Figures

Chapter 1

Introduction and Crystallography

1.1. Introduction

Magnetism and electricity are two fundamental concepts in physics and they are the foundation of the theory of electromagnetism which is defined by the four Maxwell equations. However, these two properties are usually mutually exclusive in crystals. The principle of exclusion between magnetic moment and electric dipole became not 100% true with the discovery of multiferroicity and cross coupling between electric and magnetic properties began attracting intense research interest.

1.1.1. Multiferroic and magnetoelectric materials

By the original definition of Schmid in 1994, multiferroic materials simultaneously exhibit more than one primary ferroic order parameters in a single phase [1]. Four primary ferroic order moments are a magnetic moment, an electric dipole moment, an elastic moment and a magnetic toroidal moment. In general, a magnetic moment breaks the time-reversal symmetry (a system does not change if the flow of time is reversed) and spontaneous behavior of it in matter leads to a ferromagnetic ordering. On the other hand, an electric dipole moment breaks the space-inversion symmetry (a system does not change if the position is reversed) in matter which leads to ferroelectric order. An elastic moment does not break any of these two symmetries mentioned above but comes from lattice distortion. In contrast, a magnetic toroidal moment breaks both the time-reversal and the space-inversion symmetries [2]. Multiferroic materials are interesting because of two main reasons: (i) the possibility of achieving functionality of both magnetic and electric orders in a one phase; and (ii) the possibility of inducing novel property from the coupling of ferromagnetic and ferroelectric states. For example, a desirable implementation would be reading and writing of magnetic bit which could reduce the waste heat and relatively long build-up time related to the electric current driven by magnetic field, if a voltage pulse is used [3].

Magnetoelectric coupling, on the other hand, does not necessarily depend on ferroic orders

and it may occur indirectly via strain or directly by coupling of two order parameters. In fact, magnetoelectric (ME) effect is the phenomenon that induces electric polarization by externally applying a magnetic field in matter *or vice versa* (i.e. induces magnetization by applying an electric field).

1.1.2. Brief History

The history of ME effect dates back to the late 19th century to Pierre Curie's paper about the prediction of possible intrinsic ME effect in some crystals [4], while the term "magnetoelectric" was first defined by Debye in 1926 [5]. However, these were not successful attempts to demonstrate ME effect until Landau and Lifshitz further advanced the concept and formulated the mathematical expression of linear ME effect and realizing that ME response is only allowed if there is a breaking in both the time-reversal and the space-inversion symmetries [6]. Hence, Gibbs free energy density of a ME material can be expressed as:

$$E(\boldsymbol{\mathcal{E}}, \boldsymbol{H}) = E_0 - \frac{1}{2}\epsilon_0\epsilon_{ij}\mathcal{E}_i\mathcal{E}_j - \frac{1}{2}\mu_0\mu_{ij}H_iH_j - \alpha_{ij}\mathcal{E}_iH_j - \dots \tag{1.1}$$

where i and j label Cartesian directions, ϵ_0 and μ_0 are permittivity and permeability of vacuum, and ϵ and μ are the dimensionless relative dielectric constant and permeability. Linear ME response α is defined as

$$\alpha_{ij} = \left.\frac{\partial P_i}{\partial H_i}\right|_{\boldsymbol{\mathcal{E}}} = \mu_0 \left.\frac{\partial M_i}{\partial \mathcal{E}_i}\right|_{\boldsymbol{H}} \tag{1.2}$$

where **P** is the polarization, $\boldsymbol{\mathcal{E}}$ is the electric field, **M** is the magnetization and **H** is the magnetic field.

In 1960, following Dzyaloshinskii's prediction of the first ME material with linear ME effect based on its magnetic symmetry [7], the first real ME material Cr_2O_3 was discovered by measuring the magnetization which was induced by external electric field [8,9] and in the following year, experimental results about polarization induced by external magnetic field in Cr_2O_3 were

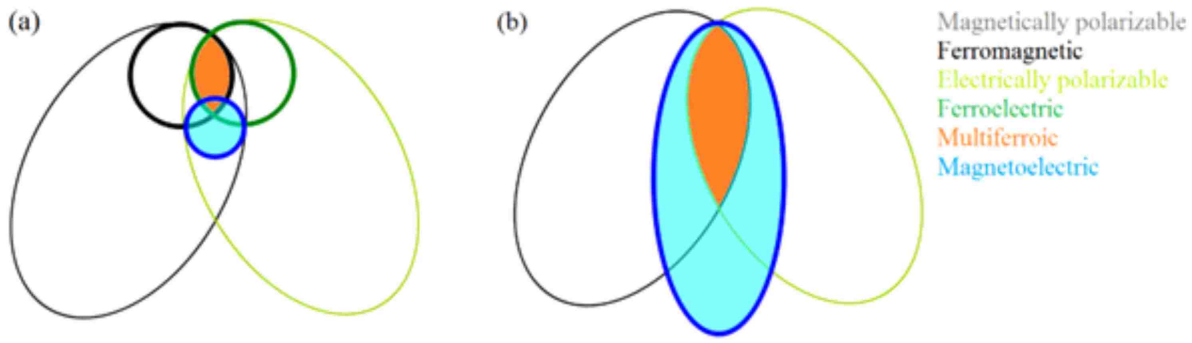

Figure 1: *A schematic landscape of multiferroic and ME materials. (a) earlier version proposed by Eerenstein, Mathur and Scott in 2006 [17]. (b) updated version proposed by Dong, Liu, Cheong and Ren in 2015 [2]. The figure is reproduced from Ref. [2]*

reported [10,11]. Then the idea of achieving cross coupling of magnetic and electric properties started to generate an intense research interest. However even after decades of effort, there were still few available ME materials and observed ME response was small, and on the other hand, the microscopic understanding of ME effect was limited and the absence of elements from the modern electronic theory hindered the further development of the field.

This gradual pace continued till two unexpected breakthroughs that happened in 2003, following the influential paper containing a question "Why are there so few magnetic ferroelectrics?" in 2000 [12]. The first new multiferroic material was $BiFeO_3$ which is a room-temperature ferroelectric with a notable magnetization [13] and the second one was orthorhombic $TbMnO_3$ with intrinsically exhibits a strong ME coupling, which enabled flipping of polarization by a magnetic field [14]. And the next year, two new multiferroic materials were discovered as well: orthorhombic $TbMn_2O_5$ [15] and hexagonal $HoMnO_3$ [16]. After observation of novel ME coupling mechanisms in these new multiferroic materials, the term "multiferroic" was expanded to include new terms such as antiferromagnetism and ferrimagnetism. Since then, the revival of the research interest in the ME effect has been enormous and there is a huge number of reports of novel multiferroic materials and ME coupling effects, which are making the microscopic mechanism of ME more understandable and establishing a new framework of multiferroicity. In 2006, Eerenstein *et al.* proposed a landscape of ME and multiferroic materials [17] that is schematically shown in Fig.

1(a), but with all the new findings since 2003, the terminology "multiferroic" is expending even more and it is illustrated in Fig. 1(b) [2].

1.1.3. Mechanism

The microscopic mechanism behind the coupling between charge and spin in multiferroic and ME materials is very fascinating and there are various types of mechanism of multiferroicity because of diverse possible origins of ferroelectricity. Possible origins of ferroelectricity may be driven by electronic lone pairs, magnetism (spin), charge order or geometric effects. Multiferroic materials are divided into two groups: (i) type-I multiferroics which have ferroelectricity driven by electronic lone pairs, polar instabilities, charge order or geometric effect, and orders of ferroelectricity and magnetism take place independent of each other; (ii) type-II multiferroics which have ferroelectricity driven by magnetism and ME phenomena emerge jointly. A well-known example of type-I multiferroic is $BiFeO_3$ and it is intensely studied due to its prominent ferroelectricity above room temperature which allows a manipulation of ferroelectric domains and possible control of magnetism by an electric field. On the other hand, an example of type-II multiferroic is $TbMnO_3$ and it is actively studied due to its significance of physics (microscopic ME mechanism) rather than its application. However, ME effect does not only exist in multiferroics and in fact, the first discovered ME material Cr_2O_3 is not multiferroic.

So far, there are three main types of spin-induced ferroelectric mechanisms that can give rise to a ME effect and they are the inverse Dzyaloshinskii-Moriya (DM) interaction, exchange striction, and spin-dependent p-d hybridization. In general, these mechanisms can be divided into two groups based on whether it has the influence of spin-orbit coupling or not. DM interaction promotes a relativistic correction to the exchanges in the presence of spin-orbit coupling (antisymmetric magnetic interaction) [18–21]. If we take into account a perovskite ABO_3 structure, then bending of B-O-B bond away from its centrosymmetric angle of 180°, will induce DM interaction as a relativistic correction. The Hamiltonian of this interaction can be expressed as follows:

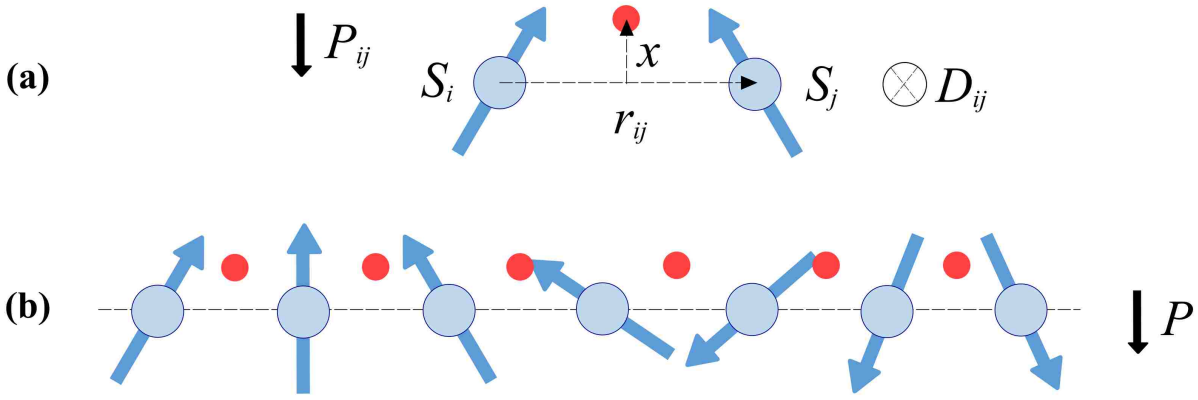

Figure 2: *The Dzyaloshinskii-Moriya interaction*

$$H_{DM} = \sum_{i,j} \boldsymbol{D}_{ij} \cdot (\boldsymbol{S}_i \times \boldsymbol{S}_j) \tag{1.3}$$

where $\mathbf{D}_{ij}$ is the coefficient of the DM interaction between spins $\mathbf{S}_i$ and $\mathbf{S}_j$, as shown in Fig. 2(a). The Dzyaloshinskii vector **D**ij is proportional to the displacement (shift) **x** of oxygen ion away from the middle point of the ij bond

$$\boldsymbol{D}_{ij} \sim \boldsymbol{x} \times \boldsymbol{r}_{ij} \tag{1.4}$$

where $\mathbf{r}_{ij}$ is the vector pointing from site i to site j. Since DM interaction promotes non-centrosymmetric structure, magnetic interaction becomes antisymmetric which leads to a non-collinear spins. In a non-collinear magnetic structure, oxygen ions move off-center to gain DM energy and generate a local electric dipole

$$\boldsymbol{P}_{ij} \sim \boldsymbol{r}_{ij} \times (\boldsymbol{S}_i \times \boldsymbol{S}_j) \tag{1.5}$$

In the inverse DM interaction, a cycloidal spin structure drives a non-centrosymmetric displacement of charges, as shown in Fig. 2(b). Therefore, all the oxygen ions shift at the same direction with a macroscopic polarization which is coupled with its acentric spin structure.

In contrast to DM interaction, there is the exchange striction which is described by following Heisenberg model:

$$H_{ME} = \sum_{i,j} J_{ij}(\boldsymbol{S}_i \cdot \boldsymbol{S}_j) \tag{1.6}$$

where J is exchange integral and spins at site i and j are S_i and S_j. J depends on the length and angle of the bridge between magnetic cations through the anion. Symmetric spin product $\boldsymbol{S}_i \cdot \boldsymbol{S}_j$ derives an acentric displacement of charges. This kind of ferroelectricity was first observed in $TbMn_2O_5$ [22] and this mechanism does not depend on spin-orbit coupling as well as it is not restricted to non-collinear magnetic ordering.

Finally, spin-dependent metal-ligand hybridization is another type of mechanism that depends on spin-orbit coupling. Delafossite compounds, such as $CuFeO_2$, are reported to have spontaneous polarization induced by their screw-like spin structure.

1.1.4. Application

The quest for new materials with a strong coupling of magnetic and electric properties is still going strong in the field of multiferroic since the 1960s. Specially, a room-temperature multiferroic with a strong coupling between magnetization and polarization remains a prime goal. While with the advances in the field, some ME composites are already being used in many prototype devices and integrated systems such as memories, magnetic sensors, magnetoelectric transducers, tunable microwave devices, etc. [23]. Most important achievements would be a reversal of magnetization by the electric field in $BiFeO_3$-CoFe heterostructure [24] and low-temperature four state memory concept on multiferroics [25]. Multiferroic materials continue to reveal novel physics of ME coupling and extent of its application is growing far beyond the electric control of magnetism.

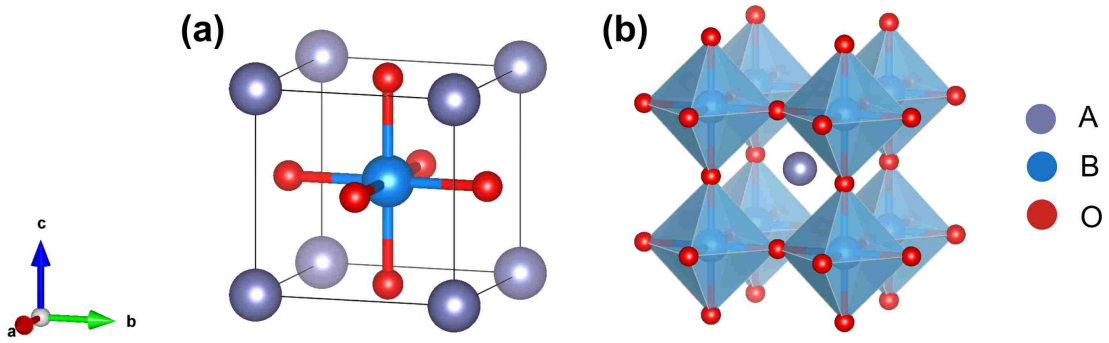

Figure 3: *Schematic plot of ABO_3 perovskite structure. (a) The unit cell of an ABO_3 perovskite with a cubic crystal structure. (b) BO_6 polyhedrons are shown with A cation in the center.*

1.2. Perovskite structure

A family of compounds called perovskites refers to a mineral of formula $CaTiO_3$ which is the first of its family that has been discovered in 1839 and named after Russian mineralogist L. A. Perovski. The general formula is ABX_3, where A is usually a larger cation, B is usually a smaller cation and X is an anion. As of today, there are many compounds that are known to adopt perovskite structure. Particularly, ABO_3 perovskite oxides from a very important family of ferroelectric materials and the first ferroelectric oxide is $BaTiO_3$. At high temperature, the Bravais lattice is simple cubic and the basis has five atoms: A atom at (0,0,0), B atom at (1/2,1/2,1/2) and three oxygen atoms at (1/2,1/2,0), (1/2,0,1/2) and (0,1/2,1/2). The overall structure is shown in Fig. 3.

The ferroelectricity in perovskite oxides is known to originate from various displacements of the ions from their highly symmetrical cubic reference points. A driving mechanism of these displacements is the subtle interaction between long-range Coulomb forces which tend to favor the ferroelectric state and short-range repulsive forces that in contrast favor the paraelectric state. Due to this mechanism, structurally similar perovskite structures exhibit a different degree of ferroelectric behavior depending on their chemical composition, pressure, strain and defects in them [26].

For example, perovskite oxides $BaTiO_3$ and $PbTiO_3$ have similar cohesive properties with a simple cubic structure (space group $Pm\bar{3}m$) at high temperature and only A site ions are different in size. However, these two perovskite oxides go through different phase transitions as temperature goes down, e.g. $BaTiO_3$ goes through three phase transitions: cubic-to-tetragonal at 393K, tetragonal-to-orthorhombic at 278K, and orthorhombic-to-rhombohedral at 183K; $PbTiO_3$ goes through only one phase transition: cubic to tetragonal at 766K.

In general, BO_6 octahedra of ferroelectric materials, as shown in Fig.3(b), make noncentrosymmetric distortion that breaks the inversion symmetry and leading to a net macroscopic electric polarization [26]. However, ABO_3 perovskite oxides are more common to make centrosymmetric distortion such as rotation and tilting of BO_6 octahedra [27].

In the case of multiferroic materials, ABO_3 transition metal perovskites have mutually exclusive ferroelectricity and magnetism and this exclusion has puzzled researchers for decades [12,28]. Apparently, the generally known phenomenon for ferroelectric is the tendency of noncentrosymmetric distortion of the BO_6 octahedra and it requires diamagnetic ions with empty d-orbitals (known as the ferroelectric d^0 rule) but to have magnetic property there is a need for the presence of partially filled d orbitals at B site cation. Still, more and more the research effort is being focused on the design of ME multiferroic within a single-phase material due to its promising novel properties for future applications [25,29–33]. And this research made a lot of synergetic collaborations between theorists and experimentalists, and specially the modern advances of first-principles calculations are shedding a light on the physics of multiferroics.

1.3. Thin films and strain engineering

The development of state-of-the-art thin film deposition tool also made a huge impact in the field of multiferroics. In fact, one of the groundbreaking findings of 2003, $BiFeO_3$ was a thin film grown by pulsed laser deposition technique [13]. However, careful tuning of synthesis condition is one of the keys to having enhanced multiferroic properties in a thin film with respect to the bulk counterpart. With successful thin films growth, some extrinsic properties can be introduced to the

system such as substrate-induced strain, impurity states, surface states, structural defects, etc.

Generally, the first step of synthesizing thin films is selecting the right substrates. Therefore, to have a minimum amount of structural defects requires a good lattice match between the film and the substrate but making lattices mismatch with each other is also a good way to optimize physical properties of the material [34]. This lattice mismatching technique is referred as strain engineering and strain (either tensile or compressive) engineering can enhance spontaneous polarization and Curie temperature of ferroelectric oxides [35]. Likewise, the properties of multiferroic thin films can also be modified by the epitaxial strain. For example, compressive strain on the tetragonal phase of $BiFeO_3$ with a c/a value of more than 1.25 is reported to possess a spontaneous polarization up to 150 $\mu C/cm^2$ [36–39].

Strain can change, by a considerable amount, the phase diagram of strongly correlated oxides within multiple degrees of freedom. For instance, in a system with a strong spin-phonon coupling, strain can induce a phase transition from an antiferromagnetic-paraelectric to ferromagnetic-ferroelectric state due to polar instability if the lowest-optical polar phonon mode is softer for the ferromagnetic arrangement. In fact, this strain-induced multiferroic state was predicted by first-principle calculation results of $SrMnO_3$ [40] and similar strain-mediated multiferroic states of $CaMnO_3$ was also predicted [41]. Moreover, strain can be used to couple ferromagnetic and ferroelectric domains across an interface by means of magnetoelectric and magnetostrictive couplings [42,43].

1.4. Motivations and goal of the research

The d^0 rule for ferroelectricity in perovskite oxides was first observed by Matthias almost 70 years ago [44]. As explained in the section 1.2, this Matthias rule is problematic for multiferroic materials because of the fact that magnetism requires unpaired d^n cations. However, a violation of this rule was first predicted for $BaMnO_3$ and epitaxially strained $CaMnO_3$ films [41,45]. The polar ground state for the non-d^0 magnetic cations was the result of off-centering distortion due to the second order Jahn-Teller distortion mechanism. In general, when B-O bond length of magnetic

ions like Mn^{4+} or Fe^{3+} becomes long enough, the central magnetic ion position becomes unstable and a spontaneous off-centering is preferred to lower the energy of the system. There are two possible ways to stretch the B-O bond length long enough: (i) use the epitaxial strain from the substrate; (ii) use a big ion at the A-site to create negative pressure. The best candidate to try the second route is $BaMnO_3$ and it was predicted to have a polarization of 12 $\mu C/cm^2$ but unfortunately, the perovskite structure in this compound is unstable. To address this issue, Sakai *et al.* did partial substitution of Ba by Sr atoms to stabilize the perovskite structure [46]. Indeed, they have reported that the perovskite structure of $Sr_{1-x}Ba_xMnO_3$ with x>0.4 became stable and ferroelectric with a polarization of 4.5 $\mu C/cm^2$ [46,47]. Results are summarized in Fig. 4 and $Sr_{0.5}Ba_{0.5}MnO_3$ was found to be multiferroic.

Later, a theoretical prediction was done on the $Sr_{1-x}Ba_xMnO_3$ system as a function of chemical doping, external pressure and epitaxial strain in 2016 [48]. Here, the multiferroic $Sr_{0.5}Ba_{0.5}MnO_3$ (SBM) alloy was reported to go through a first-order magnetic phase transition from antiferromagnetic to ferromagnetic when enough tensile strain is introduced to the system.

Now, let us discuss the effect of strain on the d^0 ferroelectricity. One good example would be the recently synthesized super-tetragonal $BiFeO_3$ thin films [36]. There, a giant ferroelectric polarization was observed along the c-axis regardless of the d^5 nature of Fe ion, due to the extremely elongated Fe-O bonds along their c-axis.

Therefore, there are several questions one could wonder: Is it possible to achieve a giant ferroelectric polarization, like in super-tetragonal $BiFeO_3$, by introducing compressive strain into the multiferroic SBM system? Is it possible to induce a first-order magnetic phase transition from antiferromagnetic to ferromagnetic via compressive strain like it was reported to happen in the tensile strain region? If so, does this magnetic phase transition enhance polarization and c/a value, which could lead to a large magnetoelectric coupling? Especially, is it possible to fulfill one "goal" in the fields of multiferroics, that is to discover a strongly polar material with a ferromagnetic arrangement, and with properties that are controllable by an external factor [49]? Another question to resolve and that is possible with strain engineering is to know if playing with strain can create an-

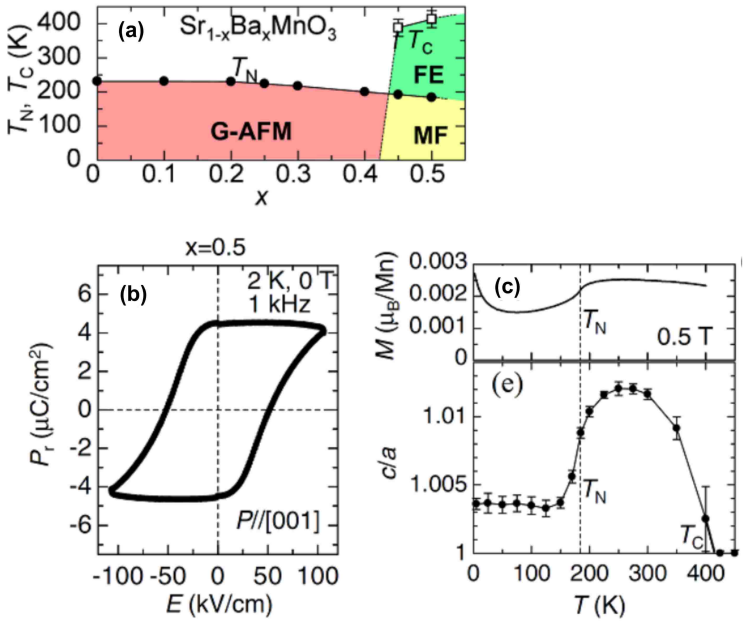

Figure 4: *Sakai et al. results [46]. (a) Phase diagram of $Sr_{1-x}Ba_xMnO_3$ as function of x. G-AFM: G-type antiferromagnetic; FE: ferroelectric; MF: multiferroic. (b) Ferroelectric P-E hysteresis loop (at 2K) along pseudocubic cubic c-axis for x=0.5 in a heavily twinned sample. (c) Temperature dependence of magnetization under 0.5 T field and c/a value.*

other phase in SBM films, namely, a low-symmetry phase bridging higher-symmetry phases such as tetragonal and orthorhombic phases in epitaxial SBM films. If such speculative low-symmetry phase exits, does it have similar physically rich properties like in some so-called morphotropic phase boundary (MPB) compounds [36,50–56]?

The goal of this thesis is to address the above-mentioned questions and, in fact, positively answer them by analyzing results obtained from first-principles calculations.

1.5. Organization of current work

The rest of the thesis is organized as follows.

We use first-principles density functional theory to calculate various physical properties of the SBM films under epitaxial strain (both compressive and tensile), such as the total energy, polarization and phonon. In Chapter 2, we give a brief introduction of the computational methods that are implemented in this work and cover basic ideas of the density functional theory. In addition, we

explain concisely the meaning of phonons and the computational approach to study polarization.

In Chapter 3, we present the *ab-initio* calculations results predicting novel physical properties of SBM films under epitaxial compressive and tensile strains. Using first-principles density functional methods, we calculate the total energy of four different magnetic configurations (G-type antiferromagnetic, A-type antiferromagnetic, C-type antiferromagnetic and ferromagnetic [57]) of SBM films in a large range of epitaxial strain. Then, using the Berry phase method [58], we calculate the electronic polarization of all four magnetic configurations within all regions of epitaxial strain and, using the Isotropy software [59], we identified the space groups of all structures. Also, we performed phonon calculations to further investigate the unusual physical property of the specific region of epitaxial strain.

Lastly, in Chapter 4, we summarize our work and point out some further investigations regarding the magnetoelectric coupling in epitaxial SBM films.

Chapter 2

Computational methods

For a solid that consists of ion cores and valence electrons, solving the exact total Hamiltonian is nearly impossible with current computational capability, because the exact solution would involve treating a quantum number of the order of $\sim 10^{23}$ and the Coulomb interaction between electrons in the system. Therefore, we must take an account of approximation from the start to solve this many-electron problem.

In this chapter, we give a brief introduction to the density functional theory (DFT), which is one of the widely used first-principles approaches to solve the above mentioned many-body problem in many disciplines ranging from physics to chemistry via materials science and more. Furthermore, we also briefly discuss the computational methods for phonons and polarization calculations.

2.1. Density Functional Theory

2.1.1. Hohenberg-Kohn theorems

Density functional theory is based on the two Hohenberg-Kohn theorems that were published in 1964 [60]. The first and most important one states that, for a many-electron system, the ground state electron density n(r) uniquely determines, the total energy of the ground state. With this theorem, one can write the Hamiltonian of many-electron system as a functional of the ground state electron density and different many-electron systems will differ only by the local external potential energy V(r) acting on the electrons. Then, separating the interaction with V(r) from the total energy, the ground-state energy can be written as

$$E_v[n] = \int V(r)\, n(r)\, dr + F[n] \tag{2.1}$$

where n(r) is the electron density and F[n] is the universal functional of the density which is independent of V(r). The second theorem states that for any system (that is, for any V(r)), the total

energy $E_V[n']$ of any arbitrary density n'(r) will always be greater or equal to that of the ground state energy:

$$E_v\left[n_0\left(r\right)\right] \leq E_v\left[n^{'(r)}\right] \tag{2.2}$$

In other words, the correct ground state density always minimizes the energy functional in Eq. 2.1. Hohenberg-Kohn further noted that, for nonrelativistic Coulomb systems, the kinetic energy and interaction energy between electrons are universal and only depend on the density. Therefore, the ground state energy can be written as a unique functional of the ground state charge density:

$$E_0 = E\left[n_0\left(r\right)\right] = \langle \psi\left[n_0\left(r\right)\right] | T + U_{ee} + V\left[n_0\left(r\right)\right] | \psi\left[n_0\left(r\right)\right] \rangle \tag{2.3}$$

where T is the total kinetic energy, U_{ee} is the electron-electron interaction energy and V is the interaction energy with the external potential. However, in practice, the exact forms of the functionals of T and U_{ee} are unknown and the use of approximation is crucial for finding the ground state energy.

2.1.2. Kohn-Sham equations

One year later, an approximation was introduced by Kohn and Sham to formulate the energy functional [61]. The basic idea was to assume the interaction many-body system as a fictitious non-interacting system and take the charge density n(r) of the interacting system as the sum of densities of the N non-interacting electrons:

$$n\left(r\right) = \sum_{i}^{occ} \left|\psi_i\left(r\right)\right|^2 \tag{2.4}$$

where ψ_i is the wavefunction of the non-interacting electrons. Now, if we take into consideration the Hohenberg-Kohn theorems, then non-interacting wavefunction ψ_i is also a functional of the non-interacting density. Therefore, the density functional will be

$$E_{KS}\left[n\right]=-\frac{\hbar^2}{2m}\sum_i\left\langle\psi_i|\nabla^2|\psi_i\right\rangle+\int V_{ext}\left(\boldsymbol{r}\right)n\left(\boldsymbol{r}\right)d\boldsymbol{r}+\frac{e^2}{2}\iint\frac{n\left(\boldsymbol{r}\right)n(\boldsymbol{r}')}{|\boldsymbol{r}-\boldsymbol{r}'|}d\boldsymbol{r}d\boldsymbol{r}'+E_{xc}\left[n\left(\boldsymbol{r}\right)\right] \quad (2.5)$$

where the first term is the kinetic energy of the non-interacting electrons, the second term is the potential energy of electrons in the external field created by the nuclei, the third term is the Hartree energy characterizing the classical electron-electron Coulomb repulsion, and the last term is called the exchange-correlation functional which includes all the many-body interactions. From Eq. 2.5, we can find that the density that minimizes the energy to the lowest value can be taken as the ground state density and corresponding energy as the ground state energy.

Now, applying the variational principles to the total energy functional of Eq. 2.5 and taking into consideration the orthogonality condition, one can write a set of N single electron equations that are known as Kohn-Sham equations:

$$\left[-\frac{\hbar^2}{2m}\nabla^2+V_{ext}\left(\boldsymbol{r}\right)+\int\frac{e^2n\left(\boldsymbol{r}'\right)}{\left|\boldsymbol{r}-\boldsymbol{r}'\right|}d\boldsymbol{r}'+V_{xc}\left[n\left(\boldsymbol{r}\right)\right]\right]|\,\psi_i\rangle=\epsilon_i|\,\psi_i\rangle \quad (2.6)$$

where ϵ_{i} is the *i*-th eigenvalue and $\mathrm{V_{xc}}$ is the exchange-correlation potential which is expressed as

$$V_{xc}\left[n\left(\boldsymbol{r}\right)\right]=\frac{\delta E_{xc}\left[n\left(\boldsymbol{r}\right)\right]}{\delta n(\boldsymbol{r})} \quad (2.7)$$

If the explicit expression of $\mathrm{V_{xc}}$ is known, then Eq. 2.6 can be solved exactly by using self-consistent methods. Unfortunately, we do not know how to get the exact form of the exchange-correlation potential but we can still use approximations to solve Khon-Sham equations. Therefore, there are a lot of exchange-correlation functionals that are developed and it is still an ongoing trial to get best approximations to the exact solution.

2.1.3. Local density and general gradient approximation

One of the most commonly used and simplest approximations is the local density approximation (LDA) which was developed in 1981 [62]. In LDA, a non-uniform electron system is treated as a uniform electron gas and treats the exchange-correlation energy per electron at a point **r** as the one of homogeneous electron gas with the same density at point **r.** Therefore, the exchange-correlation energy can be expressed as

$$E_{xc}^{inhom}\left[n\left(\boldsymbol{r}\right)\right] \approx \int e_{xc}^{hom}\left[n\left(\boldsymbol{r}\right)\right] n\left(\boldsymbol{r}\right) d\boldsymbol{r} \tag{2.8}$$

where e_{xc}^{hom} [n(**r**)] is the exchange correlation energy per particle of the uniform electron gas with density n(**r**). However, LDA falls short when density changes rapidly as in molecules. And to fix this issue, another most widely used approximation was developed and is called the general gradient approximation (GGA). In the GGA approximation, the density gradient ∇n(**r**) is included in the exchange-correlation functional. Most commonly used GGA approximations are PW91 [63], PBE [64] and PBEsol [65]. In addition, there exists more accurate and advanced functionals which combines in the portion of the exact exchanges from Hartee-Fock theory [66].

2.2. On-Site Coulomb correction (Hubbard U and Hund J)

For transition metals with partially filled d and f electron shells, usually, both LDA and GGA fail to describe the magnetic properties of them because of the underestimation of the on-site Coulomb repulsion on the localized orbitals. Hence, two additional parameters are introduced, Hubbard U and Hund's coupling J, to better characterize the strong on-site Coulomb interactions for localized d and f electrons, and this method is called DFT+U [67,68]. Two parameters usually describe the on-site Coulomb (U) and on-site exchange (J) interactions and are mostly obtained semi-empirically. In general, if an atomic orbital is occupied by opposite-spin electrons, then Hubbard U is needed to adjust the energy difference between unoccupied orbitals and occupied orbitals. On the other hand, Hund's rule tends to maximize total spin and orbital angular momentum. In practice, there is

no surefire way to find the U and J values, and they are usually adjusted to fit experimental results or, e.g. band gap and magnetic moment.

2.3. Phonons

Crystals possess inherently dynamic lattice vibrations and collective motions of atoms at certain frequencies are called phonons. They are a quantum mechanical expression of a special type of vibrational motion in classical mechanics, known as normal modes. The normal modes are like the elementary vibrations of the lattice and are determined by the masses M and force-constant matrix

$$K_{i\alpha,j\beta} = \frac{\partial^2 E}{\partial u_{i\alpha} \partial u_{j\beta}} \tag{2.9}$$

where u is the atomic displacement and E is the total energy, and where i and j indicate atomic label, while α, β represent the three Cartesian axes. One can derive the equation of motion with respect to oscillation mode $\eta(t)$

$$\boldsymbol{M} \cdot \frac{\boldsymbol{d}^2 \boldsymbol{\eta}\,(t)}{\boldsymbol{dt}^2} = -\boldsymbol{K} \cdot \boldsymbol{\eta}\,(t) \tag{2.10}$$

If we take simple harmonic oscillation, $\boldsymbol{\eta}\,(t) = \boldsymbol{\eta}_0 e^{-\boldsymbol{iwt}}$, then Eq. 2.10 becomes

$$(\boldsymbol{K} - \boldsymbol{M}\omega^2) \cdot \boldsymbol{\eta}_0 = 0 \tag{2.11}$$

Where the phonon frequency ω and the normal mode η_0 are determined from Eq. 2.11.

When more than one atom is contained in the unit cell, the lattice will vibrate (phonon) in two different ways (types), namely acoustic and optical. In acoustic modes, ions move in synch while for optical mode, ions move in opposite directions (for zone-center modes).

2.4. Modern theory of polarization

The key to understanding ferroelectricity is correlated with the study of electric polarization. However, the microscopic understanding of polarization was problematic and it was debatable on how to calculate it from first-principles perspective, till the development of modern theory of polarization. Classically, the polarization is defined as the total dipole moment per unit volume but when it is applied to the quantum mechanical system of periodic solids, it fails to describe the polarization. For classical systems, Clausis-Mossotti (CM) model is always assumed [69]. Within the CM model, a localized electric dipole from each unit cell makes up the total charge of the periodic crystal and the electronic charge density is distributed continuously. Therefore, it is questionable to divide the charge distribution into localized contributions and use continuously distributed charge density to describe the electric dipole in a bulk crystal.

Since the concept of local electric dipole fails, there was an attempt to express polarization as the integral distribution over the unit cell divided by the cell volume:

$$\boldsymbol{P} = \frac{1}{V}\int \boldsymbol{r}\rho\left(\boldsymbol{r}\right)d\boldsymbol{r} \tag{2.12}$$

This definition could work well with the finite volume systems but it is dependent upon the size and shape of the cell, therefore it is a poor choice for infinite systems.

In order to find practical definition of polarization, it is more reasonable to study how polarization is measured in experiment. In fact, the experiment measures the current flow $\boldsymbol{j}$ during the polarization switching and the change in polarization $\Delta\mathbf{P}$ is the accumulated current flow:

$$\Delta\boldsymbol{P} = \int_0^{\Delta t} \boldsymbol{j}\left(t\right) \tag{2.13}$$

Then the spontaneous polarization $\mathbf{P}_\mathrm{s}$ is just half of the change in polarization $\Delta\mathbf{P}$. Then, the concept of the change in polarization was implemented in the new modern theory of the polarization developed by the series of papers by Resta [70,71], and King-Smith and Vanderbilt [58]. The new theory relies on the change in polarization and formulates the polarization contributed by

electrons as an integrated current across the Brillouin zone in the form of a Berry phase. Within the Berry phase approach, the Born-Oppenheimer approximation is used and polarization can be written as sum of polarization contributions from ions and electrons separately. The electronic part is more complicated and Resta [71] came to the solution of this problem by assuming that adiabatic perturbation is acting on the system and polarization is changing slowly between two different states. Then, he introduced a new parameter λ, so that when λ=0, the polarization is at its initial state and when λ=1, it is at a different state. The mathematical expression reads:

$$\Delta \boldsymbol{P_e}(\lambda) = \int_0^1 \frac{\partial \boldsymbol{P_e}}{\partial \lambda} d\lambda \tag{2.14}$$

For ferroelectric materials, λ could represent the displacement which drives the non-centrosymmetric ferroelectric displacement. For Eq. 2.14 to work, the derivative $\frac{\partial \boldsymbol{P_e}}{\partial \lambda}$ at each point along the integration should exist, requiring that the system needs to be insulating.

Then, in 1993, King-Smith and Vanderbilt [58] further simplified the above expression and pointed out that the change in polarization only depends on the initial and final states. Then, they expressed the partial derivative in Eq. 2.14 using the first-order perturbation term of Bloch wavefunctions $u(\mathbf{r})_{n\mathbf{k}}$:

$$\frac{\partial \boldsymbol{P_e}}{\partial \lambda} = \frac{ie}{8\pi^3} \int \left\langle \nabla_{\boldsymbol{k}} u_{n\boldsymbol{k}} | \frac{\partial u_{n\boldsymbol{k}}}{\partial \lambda} \right\rangle + c.c \tag{2.15}$$

where c.c. is the complex conjugate. Now, if we go to expression of the change in polarization, it can be expressed as

$$\Delta \boldsymbol{P_e} = \frac{ie}{8\pi^3} \sum_{n=1}^{occ} \int_{BZ} \langle u_{n\boldsymbol{k}} | \nabla_{\boldsymbol{k}} | u_{n\boldsymbol{k}} \rangle \, d\boldsymbol{k} \tag{2.16}$$

After we include the ionic contribution to the polarization, the total electric polarization becomes

$$\boldsymbol{P_e} = \frac{ie}{8\pi^3} \sum_{n=1}^{occ} \int_{BZ} \langle u_{n\boldsymbol{k}} | \nabla_{\boldsymbol{k}} | u_{n\boldsymbol{k}} \rangle \, d\boldsymbol{k} + \frac{e}{V} \sum_i Z_i \boldsymbol{r_i} \tag{2.17}$$

where eZ_i is the nominal charge of the ion and V is the volume of the unit cell. In practice, one does not need to integrate over the entire Brillouin zone, but rather across the mesh that reflects the symmetry of the primitive cell.

As this modern theory of polarization is expressed in terms of a geometric phase, that is the Berry phase, this theory is also called "Berry phase theory of polarization". As of today, this theory is widely used in first-principles calculations and it is a standard approach for finding bulk polarization and other properties in a weakly correlated system.

Chapter 3

Epitaxially strained $Sr_{0.5}Ba_{0.5}MnO_3$ films: Results and discussions

The magnetoelectric (ME) effect is a phenomenon for which applying an external magnetic field **H** induces polarization **P**, or applying an electric field $\mathcal{E}$ generates magnetization, as it is discussed in Chapter 1. ME effect can be either linearly or non-linearly coupled to the external applied field. The ME tensor α for linear ME effect can be decoupled into three contributions: electronic, ionic and strain mediated [72]:

$$\alpha = \alpha_{elec} + \alpha_{ion} + \alpha_{strain} \tag{3.1}$$

The electronic contribution originates from the change in the electronic polarization due to external magnetic field or *vice versa*, i.e. the change in magnetization due to the variation of electronic wavefunction under external electric field. Ionic contribution comes from the internal ionic displacement under external fields and strain contribution arises from the change in unit cell shape and volume under external fields, and therefore both ionic and strain contributions are lattice mediated. Each of these three contributions can also be decomposed into spin and orbital magnetization parts [72]. In most bulk materials, due to symmetry conditions, the strain-mediated term is mostly absent but it may not be true for thin films.

In fact, strain-induced multiferroics with both ferromagnetic and ferroelectric properties are already being experimentally proven [73], and more first-principles calculation results are predicting good candidates of new multiferroics under epitaxial strain [40,48].

In this chapter, we use first-principles density functional method to study physical properties of $Sr_{0.5}Ba_{0.5}MnO_3$ (SBM) system under epitaxial (both compressive and tensile regimes) strain.

3.1. Crystal structure

SBM bulk structure is synthesized to be tetragonal with ferroelectric distortion with an elongation of the c-axis [46]. This elongation allows magnetic Mn^{4+} ions to displace from the center of the

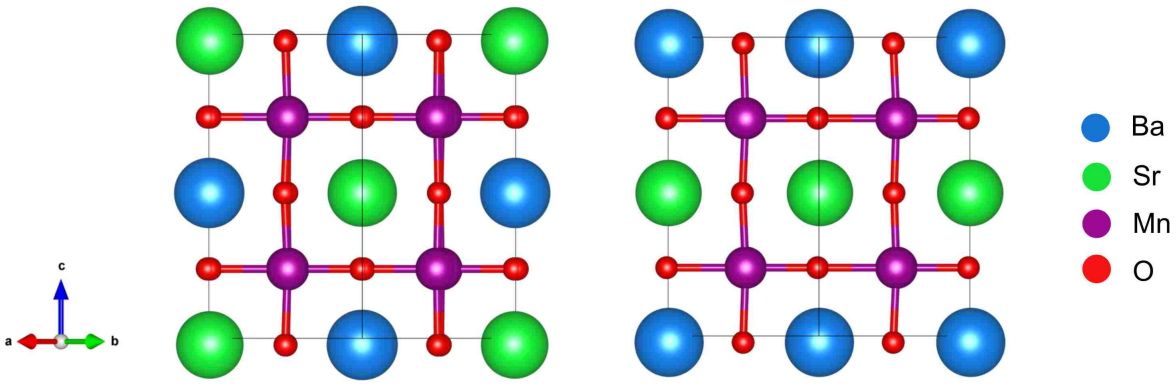

Figure 5: *Different chemical arrangements of $Sr_{0.5}B_{a0.5}MnO_3$ structures: (Left-side) Rock-salt ordered structure (DP) between its Ba and Sr atoms; (Right-side) Layered structure made of Ba and Sr atom layers (DL)*

surrounding oxygen octahedron, leading to a ferroelectric phase. Experimentally determined space group is *P4mm,* in-plane lattice constant a_{ip}=3.85Å with c/a value of 1.0035 at low temperature. The magnetic ground state is determined to be G-type antiferromagnetic.

In this study, we considered two different chemically-ordered structures since it is beyond the current reach of first-principles calculations to mimic chemically-disordered system because it would require a huge number of atoms and very big supercells. These two different chemically-ordered structures are arranged in a way that one exhibits rock-salt ordering (RS) between its Ba and Sr atoms, a similar to Refs [48,74–76], while the other possesses alternating (001) layers made of Ba or Sr atoms. These two structures are denoted as "DP" (for double perovskites) and "DL" (for double layers), respectively, and are depicted in Fig. 5.

Furthermore, we considered four commonly found magnetic orderings in manganites, which are G-type antiferromagnetic (G-AFM), A-type ferromagnetic (A-AFM), C-type antiferromagnetic (C-AFM), and ferromagnetic (FM) [57]. These specific types of orderings are illustrated by Eric Bousquet and Andres Cano in Ref. [77] and are shown in Fig. 6.

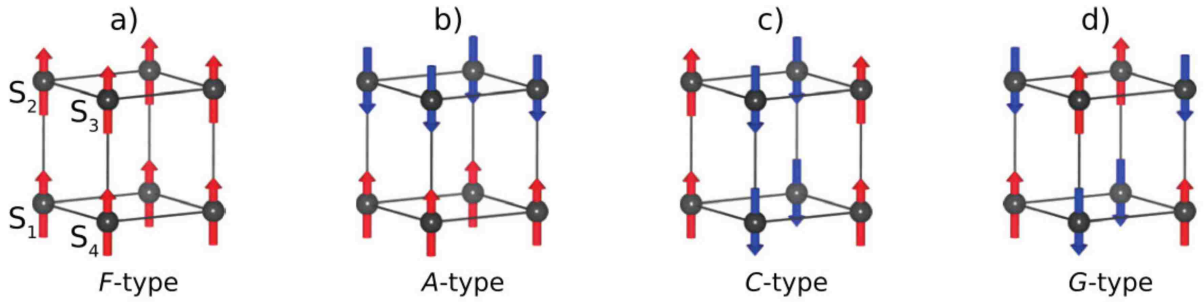

Figure 6: *Schematic view of collinear magnetic orders: (a) ferromagnetic FM, (b) A-type antiferromagnetic, (c) C-type antiferromagnetic, and (d) G-type antiferromagnetic [76].*

3.2. Computational details

For all calculations, strain was introduced to the first-principles density functional method by freezing the in-plane lattice parameter a_{ip} and the in-plane lattice vectors but allowing all other structural degrees of freedom, including the out-of-plane lattice parameter and atomic positions, to relax the structure and lower the total energy until residual forces are smaller than 0.001 eV/Å. Chosen in-plane lattice parameters range between 3.78Å to 4.11Å. All first-principles DFT calculations are carried out by the Vienna *ab initio* simulation package (VASP) [78]. The ionic core environment is simulated by the projector augmented-wave potentials [79]. For the exchange-correlation functional, we have chosen the PBE+U+J functional [64,68] and the Hubbard U value on Mn atoms is selected to be 2.0 eV, 3.0 eV or 4.5 eV (in order to check the influence of U on physical properties) while the Hund J value is taken to be 1.0 eV, as similar to Ref. [75]. We use a $\sqrt{2} \times \sqrt{2} \times 2$ simulation cell that has 20 atoms to adapt four different magnetic orderings that are previously mentioned, and an energy cutoff of 550 eV is used along with a $6 \times 6 \times 4$ Monkhorst-Pack k-point mesh. The Berry phase method [58] is used to calculate the polarization and space groups are identified using the Isotropy software [59]. Moreover, phonon frequencies are computed at the Γ-point of the supercell from the Hessian matrix via finite difference method within the DFT package.

In addition, we also used the PBEsol functional [65] with Hubbard U corrections (with U = 2 eV, 3 eV, 4.5 eV) and Hund J=1.0 eV to compute properties of epitaxial SBM films since different exchange correlation functionals can predict different results for structural and magnetic

Table 1: *Influence of Hubbard U value on physical properties*

Structure	Hubbard U (eV)	P^{tot} (C/m^2)	a_{ip} (Å)	c/a
DP	2	0.3517	3.8579	1.0322
	3	0.2934	3.8690	1.0219
	4.5	0.1764	3.8847	1.0076
DL	2	0.3885	3.8502	1.0426
	3	0.3114	3.8651	1.0255
	4.5	0.1436	3.8861	1.0037

properties of SBM films [48]. However, in that case, we found that the tetragonal symmetry structure that has the lowest possible energy over the whole range of investigated a_{ip} is non-polar and centrosymmetric, which contradicts the experimental finding of a polar tetragonal state with space group *P4mm* in SBM bulk [46]. Therefore, we conclude that the PBEsol functional is not appropriate to accurately mimic SBM systems.

3.3. Influence of Hubbard U and chemical ordering

First, we checked whether the choices of Hubbard U value and chemical ordering affect the physical properties of BSM bulk. In Table 3.1, we report the values of polarization, in-plane lattice constant and axial ratio of the predicted equilibrium tetragonal states of two different chemically ordered (DP and DL) structures for U = 2, 3 and 4.5 eV. Identified space groups of tetragonal phases for DP and DL structures are *I4mm* and *P4mm*, respectively, while the reported space group of the measurements in Ref. [46] is *P4mm* (because the grown sample is chemically disordered).

One can see that when increasing the U value for both the DP and DL structures: (i) polarization decreases; (ii) in-plane lattice constant increases; and (iii) and the axial ratio decreases. Now, comparing our predicted polarization values with the estimated value of 0.135 C/m^2 (which was indirectly extracted from low-temperature measurements in Ref. [46]) suggests that using U = 4.5eV (especially with the DL structure) provides the best agreement with experimental results. Similarly, if we compare our predicted c/a value with the experimentally reported c/a value of 1.003, then U = 4.5eV provides the best agreement too.

We also show the influence of Hubbard U and chemical ordering for SBM films in Fig. 7, in terms of the total energy and in-plane lattice constant. However, the results of U = 4.5eV give some incorrect results for both DP and DL configurations of the SBM films. Particularly, if we look at the orthorhombic phase minima of both DP (space group *Imm2*) and DL (space group *Amm2*) structures, which are represented by the blue dots in Fig. 7, they are of lower energy than the tetragonal states for both ordered structures and this contrasts with the reported tetragonal symmetry of the SBM bulks [46]. However, if we look at the tetragonal state minimum for lower Hubbard U values, they are lower than the minimum of the orthorhombic state in terms of energy. In other words, the energy difference between orthorhombic and tetragonal states minima is affected by the Hubbard U value for both the DP and DL configurations. Therefore, one should choose smaller U, such as 2.0 eV, to have the desired lowest state be tetragonal for both structures.

Conflict between above-mentioned results and our desire to have results which are in best agreement with the low-temperature measurements for the magnitude of the polarization in tetragonal SBM bulk [46] led us to select the intermediate 3 eV as the main concentrated value of Hubbard U for our study.

Furthermore, Fig. 7 also shows the total energy of *ferromagnetic* states of DP and DL structures as a function of in-plane lattice constant, a_{ip}, and one can see that the choice of Hubbard U is affecting the transition points at which the G-type AFM to FM magnetic phase transitions occur. Especially, if we look at lower Hubbard U value results, the magnetic phase transition point in the compressive strain region shifts left (i.e., to smaller a_{ip}) and the magnetic transition point in the tensile strain region shifts right (i.e., to larger a_{ip}) in comparison to the bigger Hubbard U value results. Also, the magnetic ground state remains G-AFM for more strains as the Hubbard U value decreases. For any U value, the DL structure needs more compressive strain than the DP structure to undergo the G-type AFM to FM transition within the tetragonal phase. Moreover, one can also see that the stable region of monoclinic phase (space group *Cm*) is becoming narrower when we increase the Hubbard U for both DP and DL structures, and it is true for both FM and G-type AFM configurations.

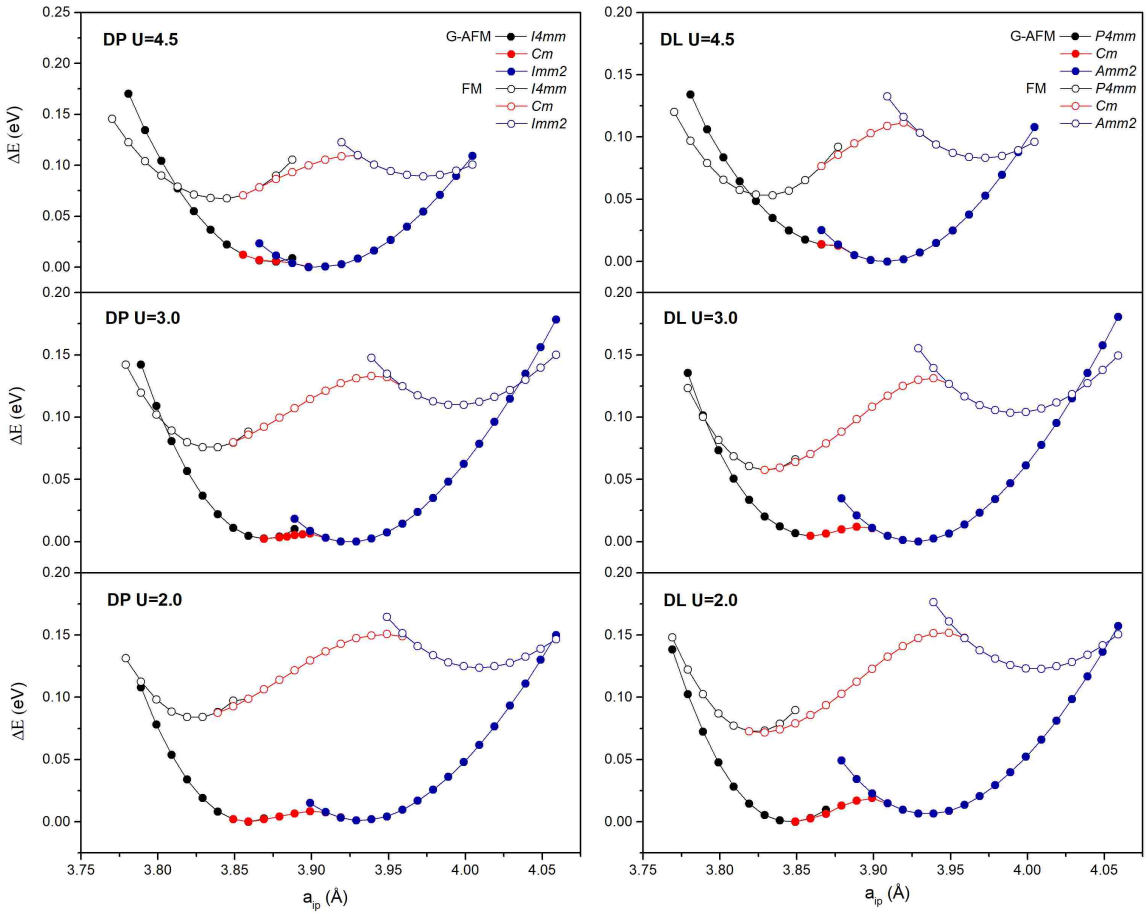

Figure 7: *Influence of Hubbard U on the total energy of the SBM films of both DP and DL arrangements using PBE+U+J functionals with U = 2.0 eV; 3.0 eV; 4.5 eV and J = 1eV as a function of the in-plane lattice constant*

3.4. Energy diagram and structural phases

Now that we choose to mainly focus on the results from a Hubbard U of 3.0 eV, Figure 8 shows the total energy as a function of the in-plane lattice constant for the four aforementioned magnetic configurations (G-AFM, C-AFM, A-AFM, and FM) and for both different chemical orderings. The results from two chemical ordering is very similar and for any of these magnetic arrangements, (1) smaller in-plane lattice constants (that correspond to compressive strains) favor the tetragonal phase; (2) larger in-plane lattice constants (that correspond to tensile strains) profit an orthorhombic phase; and (3) intermediate in-plane lattice constants result in the emergence and stabilization of

a monoclinic Cm phase. The only significant difference between DP and DL structures is the symmetry of their corresponding tetragonal and orthorhombic phases as a result of the difference in chemical ordering between Sr and Ba ions. The symmetries of the DP ordered tetragonal and orthorhombic phases are found to be *I4mm* and *Imm2*, and the corresponding symmetries of DL structures are found to be *P4mm* and *Amm2*. Interestingly, all these states are polar in nature and the *P4mm* symmetry has been previously found in chemically disordered SBM bulks [46], and atomic displacements of Mn and O atoms along the pseudo-cubic [110] direction that correspond to an orthorhombic polar state have been reported for SBM films under tensile strains [80]. However, we have not came across with any previous study reporting any monoclinic state in this system.

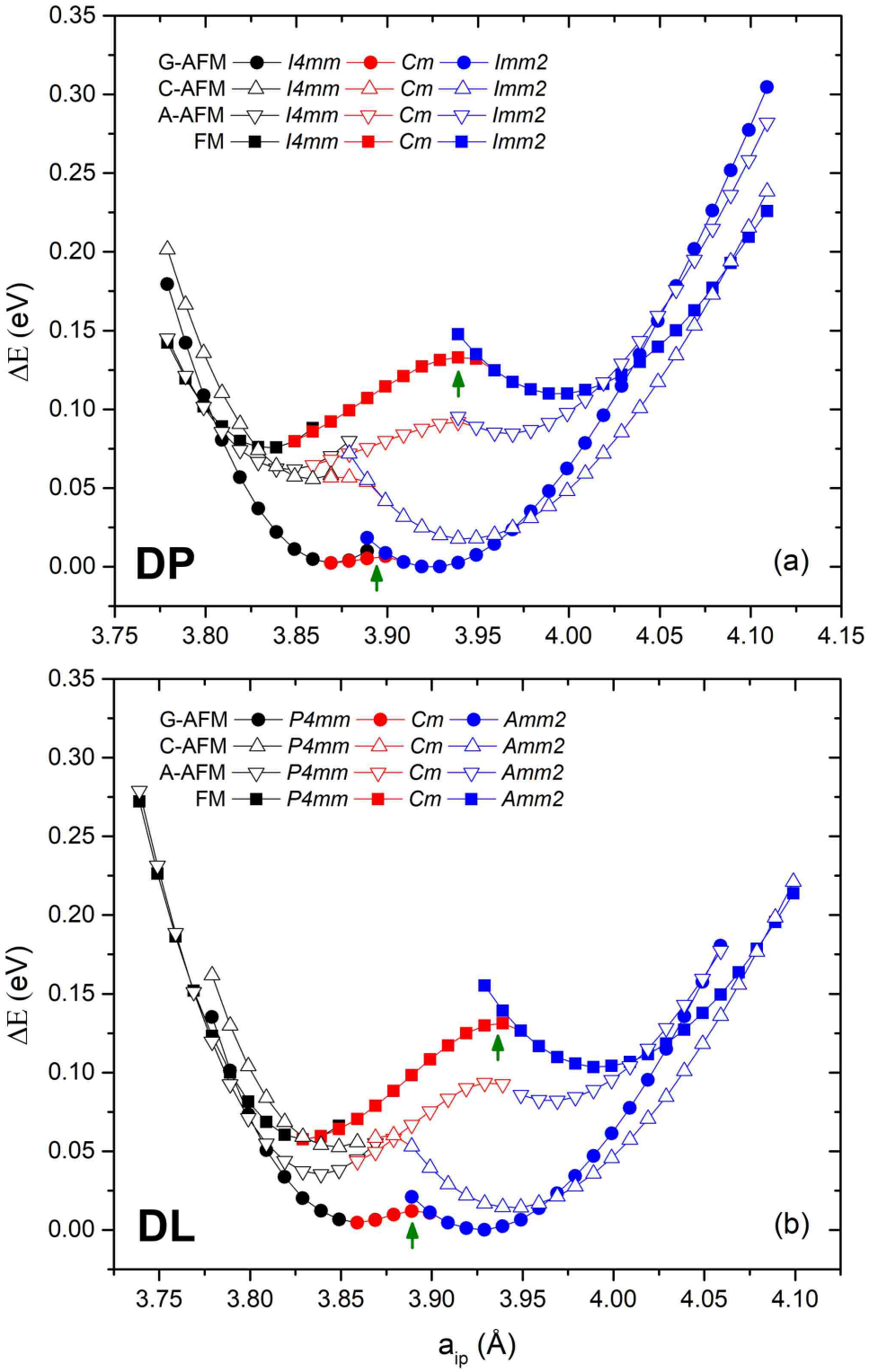

Figure 8: *The total energy as a function of in-plane lattice constants for (a) DP and (b) DL chemical orderings with the four studied magnetic arrangements. The arrows show the local maxima of the monoclinic structure for the G-AFM and FM orderings*

Furthermore, if we look at the minima of the tetragonal state and orthorhombic state of different magnetic configurations, they both strongly depend on the magnetic ordering. For example, for G-AFM and C-AFM magnetic orderings, orthorhombic state minima have lower energy than that of tetragonal state. On the other hand, the reverse is true for the A-AFM and FM magnetic orderings with lower tetragonal state minima. The total energy of the minima of the tetragonal and orthorhombic states increases by considerable amount when going from G-AFM to FM ordering, via A-AFM and C-AFM, which is consistent with Ref. [48] for SBM films under tensile strain. Therefore, the spin arrangement is strongly influencing the in-plane lattice constants corresponding to the tetragonal and orthorhombic state minima of different magnetic orderings. To further investigate above mentioned properties of SBM films under epitaxial strain, let us discuss in detail the DP structures because there is no significant qualitative difference between different chemical orderings in this system.

For instance, the minima of the orthorhombic *Imm2* state is at the in-plane lattice constant, a_{ip}, of 3.92Å for the G-AFM configuration, while it is about 4.0Å in the FM case. Similarly, a_{ip} of the tetragonal *I4mm* state minima for the G-AFM and FM configurations are 3.87Å and 3.84Å, respectively. Thus, SBM films of different magnetic orderings can have different structural states even when they have the same a_{ip}. For example, at a_{ip} = 3.92Å, the ground state associated with both G-AFM and C-AFM is orthorhombic *Imm2*, but it becomes monoclinic *Cm* for A-AFM and FM orders. Such a remarkable behavior strongly suggests that epitaxial SBM thin films grown on appropriate substrates may undergo a structural phase transition under external magnetic field, which could be a novel ME effect. As for a_{ip} = 3.92Å, one can conceive that under external magnetic field, SBM films with G-AFM orthorhombic state can become monoclinic with FM ordering. Also, if we consider the compressive strain region in Fig. 8(a), one can also envision a structural phase transition from a G-AFM tetragonal state to a FM monoclinic state at an a_{ip} of around 3.859Å. In fact, we estimated the required magnetic field to induce such structural phase transition (based on the difference of computed energies of structures for a_{ip} = 3.859Å) using Eq. 3.2:

$$\Delta E = -\mu_0 H * \mu_{tot} \tag{3.2}$$

where H is the magnetic field, μ_0 is the magnetic permeability and μ_{tot} is the total magnetic moment. We estimate the required magnetic field to be ~120T in the DP structure for a_{ip} = 3.859Å to induce the tetragonal-to-monoclinic structural phase transition. Such magnetic-field-induced phase transition would be more convincing if, as expected, with the required magnetic field should decrease in magnitude when temperature increases, since the free energies of AFM and FM states should get closer to each other when heating a magnetic system.

Another fascinating characteristic of SBM films under epitaxial strain in Figure 8, is that the magnetic ground state changes when varying the in-plane lattice constant, meaning that strain from different substrates can induce magnetic phase transitions. In fact, results from Fig. 8(a) show us that SBM films adopt a G-AFM ordering for a_{ip} between 3.80Å and 3.97Å (while the structural phase is changing from *I4mm* to *Cm*, and then from *Cm* to the *Imm2* polar states) while for a_{ip} smaller than 3.80Å, the SBM films tends to be in ferromagnetic ordering with the A-AFM order being rather close in energy (note that for the DL structure, A-AFM magnetic ordering has lower energy than FM ordering in some compressive strain region). Moreover, the SBM films tend to favor C-AFM magnetic ordering for a_{ip} larger than 3.97Å, and then adopts FM ordering for in-plane lattice constants larger than 4.09Å. Indeed, these magnetic phase transitions from G-AFM to C-AFM and then from C-AFM to FM ordering have also been reported in Ref. [48] under tensile strains but we are not aware of any study reporting strain-induced magnetic transition from anti-ferromagnetism to ferromagnetism in the SBM films under compressive strain, which corresponds to a tetragonal state region according to our calculations. Significance of this magnetic transition in the SBM films under compressive strain is followed by a rather striking feature which we will cover in the following subsection. Therefore, according to our predicted results, we suggest that growing SBM films on substrates with small lattice constants, such as the commonly used $LaAlO_3$ and $YAlO_3$ that have lattice parameters of the order of 3.7-3.8Å [81,82], should lead to observation of such ferromagnetic and tetragonal polar state of SBM films.

In order to check the accuracy of our calculations, we compared our calculation results of $SrMnO_3$ bulk with an experimental report [83] and we estimate that the presently used exchange-correlation functional PBE+U+J with Hubbard U of 3 eV and Hund J of 1 eV resulted in an overestimation of about 0.5% for the lattice constants.

3.5. Polarization

From the total energy results in Fig. 8(a) (chemical ordering is DP), one can distinguish the structural and magnetic *ground states* of the SBM films with respect to the in-plane lattice constant (i.e., strain) and they are: FM *I4mm* for in-plane lattice constants below 3.80Å; G-AFM *I4mm* for a_{ip} between 3.80Å and 3.88Å; G-AFM *Cm* for a_{ip} between 3.88Å and 3.90Å; G-AFM *Imm2* for a_{ip} between 3.90Å and 3.97Å; A-AFM *Imm2* for a_{ip} between 3.97Å to 4.09Å; and FM *Imm2* for a_{ip} larger than 4.09Å. Since all these structural symmetries are polar in nature, we show the calculated corresponding electronic polarization of these *ground states* of SBM films under epitaxial strain in Figure 9(a) as a function of the in-plane lattice constant with the vertical dashed lines representing magnetic phase transition points. Similarly, we also report in Fig. 9(b) the corresponding behaviour of the axial ratio, c/a_{ip}.

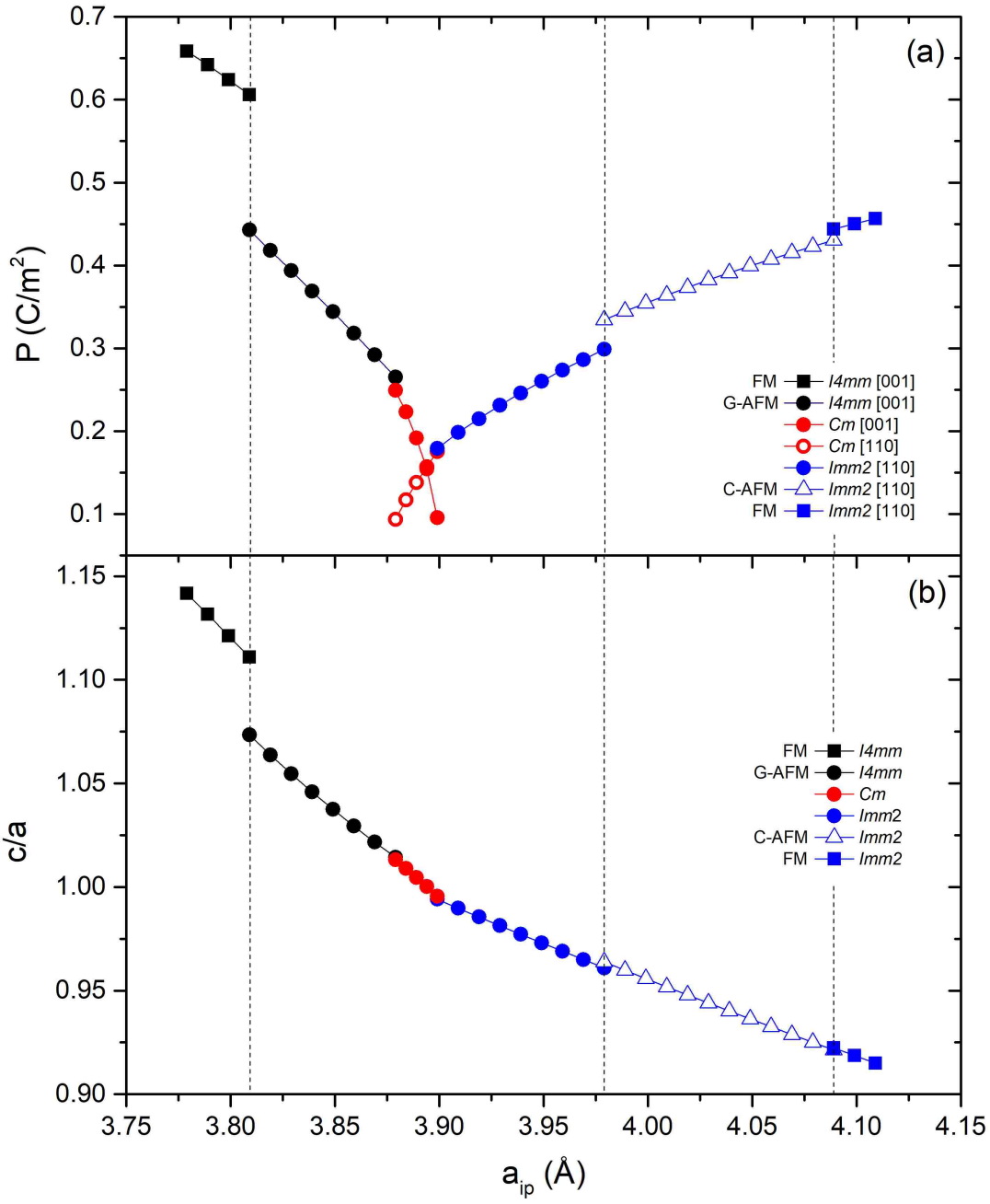

Figure 9: *Panel (a) shows the out-of-plane and in-plane components of the electronic polarization of SBM films of DP chemical ordering in the different ground states, while Panel (b) reports the associated evolution of the axial ratio. The vertical dashed lines indicate the magnetic transitions points.*

A sudden jump of both electronic polarization and c/a value can be seen in Figure 9 when SBM films go through first-order magnetic phase transitions which is an indication of a large

magnetoelectric coupling in this system under epitaxial strain. Plus, swift change in aspect ratio, when there is a change in spin configuration, hints toward significant magnetostrictive effects. Now, let us discuss in detail these huge changes in polarization and c/a values. For example, at the G-AFM to FM magnetic transition point at around a_{ip}=3.80Å, the total electric polarization jumps greatly from 0.443 C/m^2 to 0.606 C/m^2, while the axial ratio gets firmly enhanced from 1.07 to 1.11, within the tetragonal *I4mm* state. Such spin (i.e., magnetic) promoted sudden change in polarization suggests to assume an energy term of the following form in the tetragonal phase of SBM films, in order to explain such behavior:

$$\Delta E = CP_z^2(\boldsymbol{m}_1 \cdot \boldsymbol{m}_2) \tag{3.3}$$

where $P^2{}_z$ is the square of the z-component of the polarization while $\mathbf{m}_1$ is the magnetic moment averaged over every other Mn ions and $\mathbf{m}_2$ is the magnetic moment averaged over all the remaining Mn ions. Then, if we take into consideration the dot product $\mathbf{m}_1 \cdot \mathbf{m}_2$ of antiferromagnetic (which is negative) and ferromagnetic (which is positive) ordering, the *C* coefficient in this term should be *negative* with a rather strong magnitude. Note that the assumed energy term and strong, negative *C* coefficient are fully consistent with the experimental observation in Ref. [46], where the polarization and associated c/a value decrease drastically around the Néel temperature, that is when the SBM bulk undergoes a magnetic phase transition from paramagnetic (for which $\mathbf{m}_1 \cdot \mathbf{m}_2$ is essentially null, since both the averaged $\mathbf{m}_1$ and $\mathbf{m}_2$ vanish) to G-AFM within its ferroelectric tetragonal state. Furthermore, one can also see a remarkable increase of polarization when SBM films undergo a magnetic phase transition in the *Imm2* orthorhombic state, which is in the tensile strain region. The total electric polarization of the SBM film with a_{ip} around 3.98Å increases from 0.299 C/m^2 to 0.334 C/m^2 when the structure undergoes a transition from G-AFM to C-AFM magnetic state and this is fully consistent with the different magnitude of Mn off-displacement along the [110] direction found in Ref. [48] between the G-AFM and C-AFM magnetic states. This hints toward another energetic term of the form:

$$\Delta E = D(P_x^2 + P_y^2)(\boldsymbol{m}_1' \cdot \boldsymbol{m}_2') \quad (3.4)$$

where P^2_x and P^2_y are the squares of the x- and y-components of the polarization and $\mathbf{m'}_1$ and $\mathbf{m'}_2$ are magnetic moments of Mn ions that are the first-nearest neighbor of each other along the z-axis and *D* is a negative coefficient with respect to the dot product $\mathbf{m'}_1 \cdot \mathbf{m'}_2$ of both G-AFM and C-AFM magnetic states. Then, with larger tensile strain, SBM films undergo another magnetic phase transition from C-AFM to FM ordering at a_{ip} around 4.09Å with the slight increase of polarization from 0.430 C/m^2 to 0.444 C/m^2 which could be explained by an energy term similar to Eq. 3.4. In addition to the polarization changes, we can see a slight increase in the axial ratio from 0.961 to 0.964 at the G-AFM to C-AFM, and from 0.921 to 0.922 at the C-AFM to FM magnetic transitions.

Now, let us concentrate on the polar axis of different states of SBM films in Fig. 9a. In the compressive strain region where the SBM films adopt a tetragonal structure with space group *I4mm*, its polar axis lies along the pseudo-cubic out-of-plane [001] for which the c value increases when a_{ip} decreases (i.e., the c/a ratio increases). On the other hand, in the tensile strain region where the structure adopts orthorhombic symmetry of *Imm2* space group, the polar axis is along the pseudo-cubic [110] direction with c/a decreases as a_{ip} increases. These two polar axes are commonly observed in perovskite films such as $PbTiO_3$ films [54]. On the other hand, let us discuss the polarization axis of the newly found, low-symmetry monoclinic region that bridges the two high-symmetry structures of tetragonal and orthorhombic states. This monoclinic region adopts the space group *Cm* which is also a subgroup of both *I4mm* and *Imm2*. As it is shown in Fig. 9, the polar axis of the monoclinic region rotates continuously between the pseudo-cubic [001] and [110] directions, along with a steady decrease of its axial ratio from 1.01 to 0.99 when increasing the in-plane lattice constant.

3.6. Monoclinic region

The strain-induced polarization axis rotation and steady change in axial ratio is predicted in the SBM films, and it is an evidence of a rather very important property, that is a strain-induced morphotropic-like phase boundary existing in this system. This could lead to similar characteristics to the compositional, pressure or strain areas bridging two different high-symmetry ground states via a monoclinic state in some other perovskites (e.g., $Pb(Zr_{1-x}Ti_x)O_3$, $PbTiO_3$, $BiFeO_3$, or $(Ba_{1/2}Na_{1/2})TiO_3$-$BaTiO_3$) [50–54,84]. If we recall that such low-symmetry phases have been proven to exhibit large physical responses, such as high piezoelectricity, dielectric and elasto-optic responses [51,54–56], the currently predicted monoclinic phase is thus of high importance. Therefore, we numerically calculated the e_{33} piezoelectric coefficient of the monoclinic phase with G-AFM ordering. We chose the monoclinic structure with an in-plane lattice constant of 3.899Å and calculated the polarization by manually changing and fixing the out-plane lattice constant. Then, we used the following equation to numerically find the piezoelectric coefficient

$$e_{33} = \frac{\Delta P_z}{\Delta \sigma} \tag{3.5}$$

where P_z is z-component of the polarization and σ is strain (i.e., difference in out-plane lattice constants). The piezoelectric coefficient e_{33} is found to be as large as 16 C/m^2 which is more than four times bigger than the one predicted for the prototype ferroelectric (tetragonal) $PbTiO_3$ system [54] and about twice as large as that of the "giant-piezoelectric" (tetragonal) $0.6Pb(Mg_{1/3}Nb_{2/3})O_3$+$0.4PbTiO_3$ (PMN-PT) compound [85].

Our predicted region of monoclinic phase is in-between in-plane lattice constant of 3.88Å and 3.90Å, and if we take an account of the expected overestimation of 0.5%, the monoclinic region becomes stable from 3.86Å to 3.88Å, which interestingly matches with the pseudo-cubic lattice constant, 3.867Å, of (La,Sr)(Al,Ta)O_3 (LSAT) [86]. Therefore, it could be possible to observe such monoclinic state and its predicted large responses by growing BSM films on LSAT substrate. In fact, the perovskite phase of $Sr_{1-x}Ba_xMnO_3$ has been recently synthesized for compositions x

varying between 0.2 and 0.5 on *several* substrates, including LSAT [80].

Our predicted monoclinic *Cm* state displays another interesting behavior in Figure 8, which it does not adopt a minimum in energy as a function of a_{ip} while the tetragonal and orthorhombic states do adopt a minimum in energy as a function of a_{ip}. It rather has a local maximum and this local maximum can be seen in both chemical orderings (DP and DL) and in all four magnetic configurations. We indicated this maximum of G-AFM and FM arrangements for both DP and DL ordering in Figure 8 by green arrows. For DP structures, this maximum is located at about a_{ip} = 3.89Å and 3.94Å for the G-AFM and FM arrangements, respectively, and such local maximum has also been seen in different epitaxial films such as $PbTiO_3$ [54]. In Ref. [54], epitaxially strained $PbTiO_3$ films also have tetragonal and orthorhombic ferroelectric phases that are bridged by low-symmetry monoclinic *Cm* state and there is a rotation of the polar axis within the *Cm* phase. In fact, the polarization results of G-AFM arrangement in Fig. 9(a) show that the out-of-plane component of the polarization is smaller than its in-plane-component for a_{ip} above 3.895Å which is the in-plane lattice constant close to the maximum in Fig. 8(a). Similarly, for the FM arrangement, the in-plane component gets bigger than the out-of-plane component when a_{ip} is larger than 3.93Å, which is also the in-plane lattice constant near the maximum of the FM monoclinic phase.

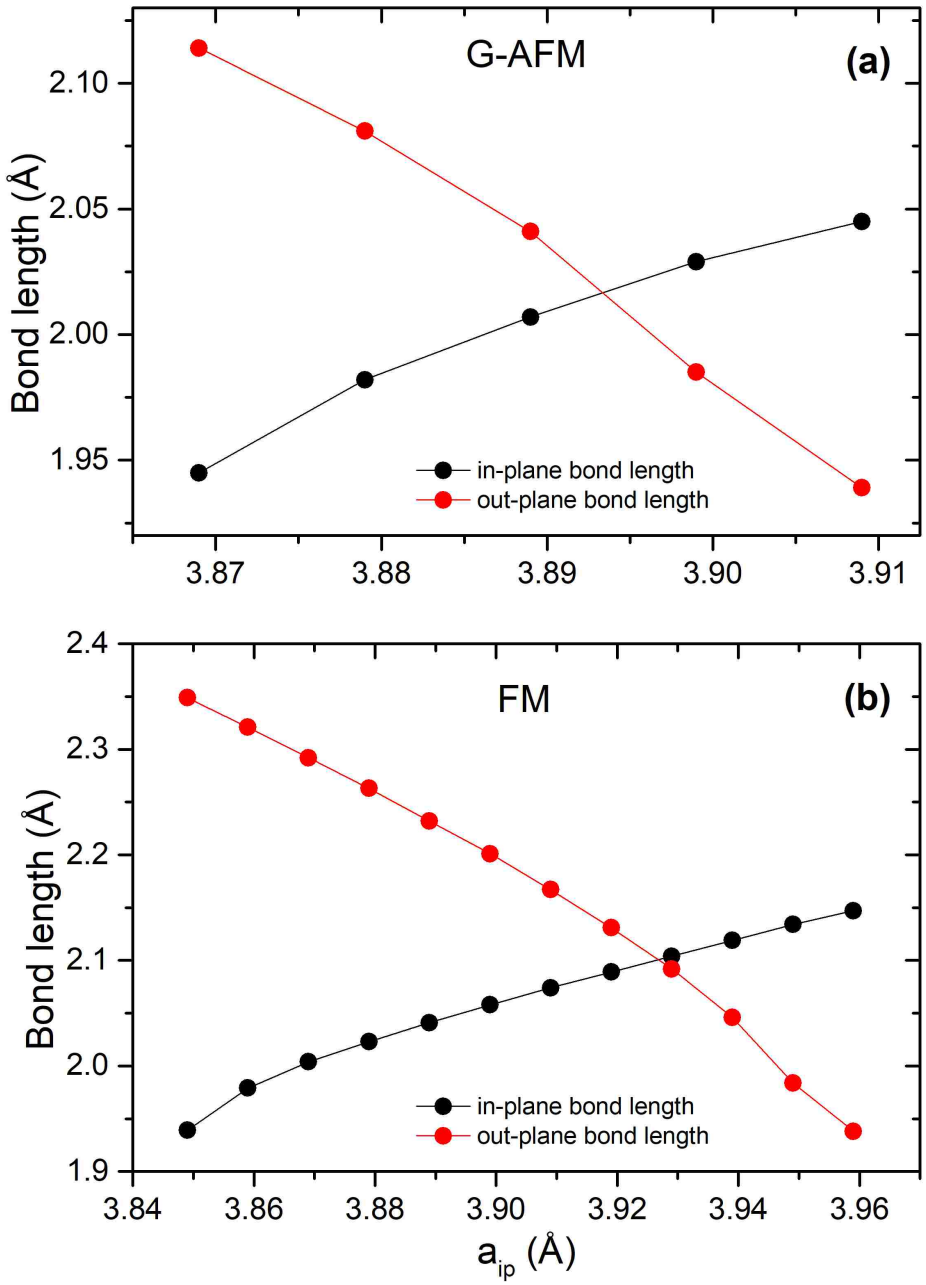

Figure 10: *Mn-O bond length of BSM films in the monoclinic phase for (a) G-AFM and (b) FM arrangements*

To further investigate this local maximum behavior of the monoclinic state, we show the bond length between Mn and O atoms in Figure 10. For both G-AFM and FM magnetic arrangements, we found the bond lengths between Mn atoms with their neighboring O atoms that reside in the

out-plane direction and the in-plane direction with respect to Mn planes. As shown in Fig. 10, the bond length of Mn atoms with their out-of-plane O atoms gets smaller than the bond length with its in-plane O atoms when a_{ip} gets larger than 3.895Å for G-AFM configuration, and similar behavior is found for the FM arrangement when a_{ip} gets larger than 3.93Å. One can thus see that the bond length results show similar qualitative behavior as the polarization results.

3.7. Phonons

We now report the computed lowest optical frequencies at the Γ-point for the G-type AFM configuration as a function of the in-plane lattice parameter in Figure 11. One can see that our predicted monoclinic state of SBM films becomes stable as the in-plane lattice constant get larger than 3.87Å and lower than 3.91Å (since the phonons in the monoclinic phase have positive frequencies). Note that

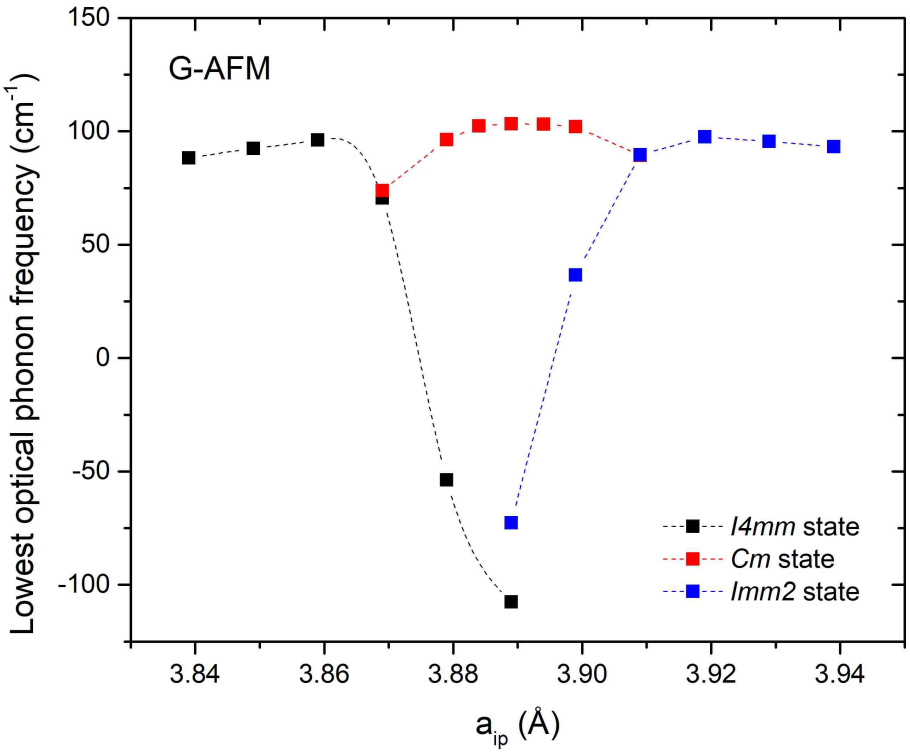

Figure 11: *The lowest optical frequencies at the Γ-point for the G-type AFM configuration as a function of the in-plane lattice parameter*

Chapter 4

Conclusion and outlook

The first-principles studies of multiferroic $Sr_{0.5}Ba_{0.5}MnO_3$ films under epitaxial strain, both in the compressive and tensile regimes, and the influence of chemical ordering in this thesis reveal several fascinating properties. In particular, this thesis shows a strain-induced magnetic phase transition from polar antiferromagnetic state to polar ferromagnetic state, followed by a huge polarization jump and axial ratio in this system, under compressive strain. Such feature strongly hints toward a realization of giant magnetoelectric coupling and magnetostriction effect. This would allow for exciting improvement in numerous devices and applications, especially since the predicted value of polarization is strong as well. In addition, one can see a strong spin-lattice coupling in SBM films because the antiferromagnetic spin arrangement (ground state) is changing when varying the in-plane lattice constant.

Another striking influence of strain in SBM films is the emergence of a strain-induced morphotropic phase boundary that is we predicted the existence of a low-symmetry monoclinic phase bridging the known tetragonal and orthorhombic states. Such monoclinic state is found to adopt a space group *Cm* that has a continuous rotation of the polarization axis within its stable region. This steady rotation of polarization axis is analyzed to be the reason of a local maximum in the energy-*versus*-in-plane lattice constant curve. With the discovery of morphotropic phase boundary, large physical response is expected and the presently found piezoelectric response is indeed as large as 16 C/m^2.

Furthermore, our calculation results predict rather unique magnetoelectric coupling effect, such as an external-magnetic-field-driven phase transition from a high-symmetry antiferromagnetic state to a low-symmetry ferromagnetic state, i.e. G-AFM tetragonal or orthorhombic state to FM monoclinic state.

All above properties may be observed since some of these predicted phenomena occur for strains that are very near to some strains induced by widely used substrates such as LSAT, $LaAlO_3$

and $YAlO_3$ [81,82,86].

Since epitaxially strained SBM films are predicted to have several interesting properties, further studies can be done to investigate deeply the magnetoelectric coupling in these systems. Possible further studies are (i) calculation of the magnetoelectric tensor α by implementing external magnetic field to first-principles calculations and look at the change in the polarization when applying different external magnetic fields; (ii) develop an effective Hamiltonian for SBM films to see what happens to currently predicted properties of epitaxial SBM films with respect to temperature and check whether the required external magnetic field to induce a structural phase transition decreases with a higher temperature; and (iii) extensive calculations of phonons around the magnetic phase transition points to get more microscopic understanding of the strong spin-phonon coupling of this system.

References

1 H. Schmid, "Multi-ferroic magnetoelectrics," *Ferroelectrics*, vol. 162, no. 1, pp. 317–338, Jan. 1994.

2 S. Dong, J.-M. Liu, S.-W. Cheong, and Z. Ren, "Multiferroic materials and magnetoelectric physics: symmetry, entanglement, excitation, and topology," *Adv. Phys.*, vol. 64, no. 5–6, pp. 519–626, Nov. 2015.

3 M. Fiebig, T. Lottermoser, D. Meier, and M. Trassin, "The evolution of multiferroics," *Nat. Rev. Mater.*, vol. 1, no. 8, p. 16046, Jul. 2016.

4 P. Curie, "Sur la symétrie dans les phénomènes physiques, symétrie d'un champ électrique et d'un champ magnétique," *J. Phys. Théorique Appliquée*, vol. 3, no. 1, pp. 393–415, 1894.

5 P. Debye, "Bemerkung zu einigen neuen Versuchen über einen magneto-elektrischen Richteffekt," *Zeitschrift für Phys.*, vol. 36, no. 4, pp. 300–301, Apr. 1926.

6 L. D. (Lev D. Landau, E. M. (Evgeniĭ M. Lifshits, and L. P. (Lev P. Pitaevskiĭ, *Electrodynamics of continuous media*. Butterworth-Heinemann, 1984.

7 I. E. Dzyaloshinskii, "On the Magneto-Electric effect in Antiferromagnetics," *JETP*, vol. 10, no. 3, p. 628, 1959.

8 D. N. Astrov, "The Magnetoelectric Effect in Antiferromagnetics," *JETP*, vol. 11, no. 3, p. 708, 1960.

9 D. N. Astrov, "MAGNETOELECTRIC EFFECT IN CHROMIUM OXIDE," *JETP*, vol. 13, no. 40, pp. 1035–1041, 1961.

10 G. T. Rado and V. J. Folen, "Observation of the Magnetically Induced Magnetoelectric Effect and Evidence for Antiferromagnetic Domains," *Phys. Rev. Lett.*, vol. 7, no. 8, pp. 310–311, Oct. 1961.

11 V. J. Folen, G. T. Rado, and E. W. Stalder, "Anisotropy of the Magnetoelectric Effect in Cr_2O_3," *Phys. Rev. Lett.*, vol. 6, no. 11, pp. 607–608, Jun. 1961.

12 N. A. Hill, "Why Are There so Few Magnetic Ferroelectrics?," *J. Phys. Chem. B*, vol. 104, no. 29, pp. 6694–6709, 2000.

13 J. Wang, J. B. Neaton, H. Zheng, V. Nagarajan, S. B. Ogale, B. Liu, D. Viehland, V. Vaithyanathan, D. G. Schlom, U. V Waghmare, N. A. Spaldin, K. M. Rabe, M. Wuttig, and R. Ramesh, "Epitaxial $BiFeO_3$ multiferroic thin film heterostructures.," *Science*, vol. 299, no. 5613, pp. 1719–22, Mar. 2003.

14 T. Kimura, T. Goto, H. Shintani, K. Ishizaka, T. Arima, and Y. Tokura, "Magnetic control of ferroelectric polarization," *Nature*, vol. 426, no. 6962, pp. 55–58, Nov. 2003.

15 T. Lottermoser, T. Lonkai, U. Amann, D. Hohlwein, J. Ihringer, and M. Fiebig, "Magnetic phase control by an electric field," *Nature*, vol. 430, no. 6999, pp. 541–544, Jul. 2004.

16 M. Fiebig, T. Lottermoser, D. Fröhlich, A. V. Goltsev, and R. V. Pisarev, "Observation of coupled magnetic and electric domains," *Nature*, vol. 419, no. 6909, pp. 818–820, Oct. 2002.

17 W. Eerenstein, N. D. Mathur, and J. F. Scott, "Multiferroic and magnetoelectric materials," *Nature*, vol. 442, no. 7104, pp. 759–765, Aug. 2006.

18 T. Moriya, "Anisotropic Superexchange Interaction and Weak Ferromagnetism," *Phys. Rev.*, vol. 120, no. 1, pp. 91–98, Oct. 1960.

19 T. Moriya, "New Mechanism of Anisotropic Superexchange Interaction," *Phys. Rev. Lett.*, vol. 4, no. 5, pp. 228–230, Mar. 1960.

20 L. Shekhtman, O. Entin-Wohlman, and A. Aharony, "Moriya's anisotropic superexchange interaction, frustration, and Dzyaloshinsky's weak ferromagnetism," *Phys. Rev. Lett.*, vol. 69, no. 5, pp. 836–839, Aug. 1992.

21 I. Dzyaloshinsky, "A thermodynamic theory of 'weak' ferromagnetism of antiferromagnetics," *J. Phys. Chem. Solids*, vol. 4, no. 4, pp. 241–255, Jan. 1958.

22 N. Hur, S. Park, P. A. Sharma, J. S. Ahn, S. Guha, and S.-W. Cheong, "Electric polarization reversal and memory in a multiferroic material induced by magnetic fields," *Nature*, vol. 429, no. 6990, pp. 392–395, May 2004.

23 J.-M. Hu, T. Nan, N. X. Sun, and L.-Q. Chen, "Multiferroic magnetoelectric nanostructures for novel device applications," *MRS Bull.*, vol. 40, no. 9, pp. 728–735, Sep. 2015.

24 J. T. Heron, J. L. Bosse, Q. He, Y. Gao, M. Trassin, L. Ye, J. D. Clarkson, C. Wang, J. Liu, S. Salahuddin, D. C. Ralph, D. G. Schlom, J. Íñiguez, B. D. Huey, and R. Ramesh, "Deterministic switching of ferromagnetism at room temperature using an electric field," *Nature*, vol. 516, no. 7531, pp. 370–373, Dec. 2014.

25 M. Gajek, M. Bibes, S. Fusil, K. Bouzehouane, J. Fontcuberta, A. Barthélémy, and A. Fert, "Tunnel junctions with multiferroic barriers," *Nat. Mater.*, vol. 6, no. 4, pp. 296–302, Apr. 2007.

26 R. E. Cohen, "Origin of ferroelectricity in perovskite oxides," *Nature*, vol. 358, no. 6382, pp. 136–138, Jul. 1992.

27 N. A. Benedek and C. J. Fennie, "Why Are There So Few Perovskite Ferroelectrics?," *J. Phys. Chem. C*, vol. 117, no. 26, pp. 13339–13349, Jul. 2013.

28 D. I. Khomskii, "Multiferroics: Different ways to combine magnetism and ferroelectricity," *J. Magn. Magn. Mater.*, vol. 306, no. 1, pp. 1–8, Nov. 2006.

29 C.-W. Nan, M. I. Bichurin, S. Dong, D. Viehland, and G. Srinivasan, "Multiferroic magnetoelectric composites: Historical perspective, status, and future directions," *J. Appl. Phys.*, vol. 103, no. 3, p. 31101, Feb. 2008.

30 J. F. Scott, "Multiferroic memories," *Nat. Mater.*, vol. 6, no. 4, pp. 256–257, Apr. 2007.

31 M. Bibes and A. Barthélémy, "Towards a magnetoelectric memory," *Nat. Mater.*, vol. 7, no. 6, pp. 425–426, Jun. 2008.

32 F. Yang, M. H. Tang, Z. Ye, Y. C. Zhou, X. J. Zheng, J. X. Tang, J. J. Zhang, and J. He, "Eight logic states of tunneling magnetoelectroresistance in multiferroic tunnel junctions," *J. Appl. Phys.*, vol. 102, no. 4, p. 44504, Aug. 2007.

33 A. Roy, R. Gupta, and A. Garg, "Multiferroic Memories," *Adv. Condens. Matter Phys.*, vol. 2012, pp. 1–12, Apr. 2012.

34 D. G. Schlom, J. H. Haeni, J. Lettieri, C. D. Theis, W. Tian, J. C. Jiang, and X. Q. Pan, "Oxide nano-engineering using MBE," *Mater. Sci. Eng. B*, vol. 87, no. 3, pp. 282–291, Dec. 2001.

35 K. J. Choi, M. Biegalski, Y. L. Li, A. Sharan, J. Schubert, R. Uecker, P. Reiche, Y. B. Chen, X. Q. Pan, V. Gopalan, L.-Q. Chen, D. G. Schlom, and C. B. Eom, "Enhancement of ferroelectricity in strained $BaTiO_3$ thin films.," *Science*, vol. 306, no. 5698, pp. 1005–9, Nov. 2004.

36 R. J. Zeches, M. D. Rossell, J. X. Zhang, A. J. Hatt, Q. He, C.-H. Yang, A. Kumar, C. H. Wang, A. Melville, C. Adamo, G. Sheng, Y.-H. Chu, J. F. Ihlefeld, R. Erni, C. Ederer, V. Gopalan, L. Q. Chen, D. G. Schlom, N. A. Spaldin, L. W. Martin, and R. Ramesh, "A strain-driven morphotropic phase boundary in $BiFeO_3$.," *Science*, vol. 326, no. 5955, pp. 977–80, Nov. 2009.

37 J. X. Zhang, Q. He, M. Trassin, W. Luo, D. Yi, M. D. Rossell, P. Yu, L. You, C. H. Wang, C. Y. Kuo, J. T. Heron, Z. Hu, R. J. Zeches, H. J. Lin, A. Tanaka, C. T. Chen, L. H. Tjeng, Y.-H. Chu, and R. Ramesh, "Microscopic Origin of the Giant Ferroelectric Polarization in Tetragonal-like $BiFeO_3$," *Phys. Rev. Lett.*, vol. 107, no. 14, p. 147602, Sep. 2011.

38 Q. He, Y.-H. Chu, J. T. Heron, S. Y. Yang, W. I. Liang, C. Y. Kuo, H. J. Lin, P. Yu, C. W. Liang, R. J. Zeches, W. C. Kuo, J. Y. Juang, C. T. Chen, E. Arenholz, A. Scholl, and R. Ramesh, "Electrically controllable spontaneous magnetism in nanoscale mixed phase multiferroics," *Nat. Commun.*, vol. 2, p. 225, Mar. 2011.

39 Z. Chen, Z. Luo, C. Huang, Y. Qi, P. Yang, L. You, C. Hu, T. Wu, J. Wang, C. Gao, T. Sritharan, and L. Chen, "Low-Symmetry Monoclinic Phases and Polarization Rotation Path Mediated by Epitaxial Strain in Multiferroic $BiFeO_3$ Thin Films," *Adv. Funct. Mater.*, vol. 21, no. 1, pp. 133–138, Jan. 2011.

40 J. H. Lee and K. M. Rabe, "Epitaxial-Strain-Induced Multiferroicity in $SrMnO_3$ from First Principles," *Phys. Rev. Lett.*, vol. 104, no. 20, p. 207204, May 2010.

41 S. Bhattacharjee, E. Bousquet, and P. Ghosez, "Engineering Multiferroism in $CaMnO_3$," *Phys. Rev. Lett.*, vol. 102, no. 11, p. 117602, Mar. 2009.

42 C.-G. Duan, S. S. Jaswal, and E. Y. Tsymbal, "Predicted Magnetoelectric Effect in Fe/$BaTiO_3$ Multilayers: Ferroelectric Control of Magnetism," *Phys. Rev. Lett.*, vol. 97, no. 4, p. 47201, Jul. 2006.

43 H. J. A. Molegraaf, J. Hoffman, C. A. F. Vaz, S. Gariglio, D. van der Marel, C. H. Ahn, and J.-M. Triscone, "Magnetoelectric Effects in Complex Oxides with Competing Ground States," *Adv. Mater.*, vol. 21, no. 34, pp. 3470–3474, Sep. 2009.

44 B. T. Matthias, "New Ferroelectric Crystals," *Phys. Rev.*, vol. 75, no. 11, pp. 1771–1771, Jun. 1949.

45 J. M. Rondinelli, A. S. Eidelson, and N. A. Spaldin, "Non-d^0 Mn-driven ferroelectricity in antiferromagnetic $BaMnO_3$," *Phys. Rev. B*, vol. 79, no. 20, p. 205119, May 2009.

46 H. Sakai, J. Fujioka, T. Fukuda, D. Okuyama, D. Hashizume, F. Kagawa, H. Nakao, Y. Murakami, T. Arima, A. Q. R. Baron, Y. Taguchi, and Y. Tokura, "Displacement-type ferroelectricity with off-center magnetic ions in perovskite $Sr_{1-x}Ba_xMnO_3$," *Phys. Rev. Lett.*, vol. 107, no. 13, pp. 1–5, 2011.

47 H. Sakai, J. Fujioka, T. Fukuda, M. S. Bahramy, D. Okuyama, R. Arita, T. Arima, A. Q. R. Baron, Y. Taguchi, and Y. Tokura, "Soft phonon mode coupled with antiferromagnetic order in incipient-ferroelectric Mott insulators $Sr_{1-x}Ba_xMnO_3$," *Phys. Rev. B*, vol. 86, no. 10, p. 104407, Sep. 2012.

48 H. Chen and A. J. Millis, "Phase diagram of $Sr_{1-x}Ba_xMnO_3$ as a function of chemical doping, epitaxial strain, and external pressure," *Phys. Rev. B*, vol. 94, no. 16, pp. 1–9, 2016.

49 H. J. Zhao, W. Ren, Y. Yang, J. Íñiguez, X. M. Chen, and L. Bellaiche, "Near room-temperature multiferroic materials with tunable ferromagnetic and electrical properties," *Nat. Commun.*, vol. 5, p. 4021, May 2014.

50 B. Noheda, D. E. Cox, G. Shirane, J. A. Gonzalo, L. E. Cross, S.-E. Park, and ., "A monoclinic ferroelectric phase in the $PbZr_{1-x}Ti_xO_3$ solid solution," Feb. 1999.

51 L. Bellaiche, A. García, and D. Vanderbilt, "Finite-Temperature Properties of $PbZr_{1-x}Ti_xO_3$ Alloys from First Principles," *Phys. Rev. Lett.*, vol. 84, no. 23, pp. 5427–5430, Jun. 2000.

52 M. Ahart, M. Somayazulu, R. E. Cohen, P. Ganesh, P. Dera, H.-K. Mao, R. J. Hemley, Y. Ren, P. Liermann, and Z. Wu, "Origin of morphotropic phase boundaries in ferroelectrics."

53 W. Jo, J. E. Daniels, J. L. Jones, X. Tan, P. A. Thomas, D. Damjanovic, and J. Rödel, "Evolving morphotropic phase boundary in lead-free $(Bi_{1/2}Na_{1/2})TiO_3$–$BaTiO_3$ piezoceramics," *J. Appl. Phys.*, vol. 109, no. 1, p. 14110, Jan. 2011.

54 L. Chen, Y. Yang, Z. Gui, D. Sando, M. Bibes, X. K. Meng, and L. Bellaiche, "Large Elasto-Optic Effect in Epitaxial $PbTiO_3$ Films," *Phys. Rev. Lett.*, vol. 115, no. 26, p. 267602, Dec. 2015.

55 L. Zhang, M. Zhang, L. Wang, C. Zhou, Z. Zhang, Y. Yao, L. Zhang, D. Xue, X. Lou, and X. Ren, "Phase transitions and the piezoelectricity around morphotropic phase boundary in $Ba(Zr_{0.2}Ti_{0.8})O_3$-$x(Ba_{0.7}Ca_{0.3})TiO_3$ lead-free solid solution," *Appl. Phys. Lett.*, vol. 105, no. 16, p. 162908, Oct. 2014.

56 A. Prasatkhetragarn, N. Vittayakorn, S. Ananta, R. Yimnirun, and D. P. Cann, "Synthesis and Dielectric and Ferroelectric Properties of Ceramics in (1-x)Pb($Zr_{1/2}Ti_{1/2}$)O_3–(x)Pb($Co_{1/3}Nb_{2/3}$)O_3 System," *Jpn. J. Appl. Phys.*, vol. 47, no. 2, pp. 998–1002, Feb. 2008.

57 E. O. Wollan and W. C. Koehler, "Neutron Diffraction Study of the Magnetic Properties of the Series of Perovskite-Type Compounds [(1-x)La, x Ca]MnO_3," *Phys. Rev.*, vol. 100, no. 2, pp. 545–563, Oct. 1955.

58 R. D. King-Smith and D. Vanderbilt, "Theory of polarization of crystalline solids," *Phys. Rev. B*, vol. 47, no. 3, pp. 1651–1654, Jan. 1993.

59 H. T. Stokes and D. M. Hatch, "FINDSYM: program for identifying the space-group symmetry of a crystal," *J. Appl. Cryst. J. Appl. Cryst*, vol. 38, no. 18, pp. 237–238, 2005.

60 P. Hohenberg and W. Kohn, "Inhomogeneous Electron Gas," *Phys. Rev.*, vol. 136, no. 3B, pp. B864–B871, Nov. 1964.

61 W. Kohn and L. J. Sham, "Self-Consistent Equations Including Exchange and Correlation Effects," *Phys. Rev.*, vol. 140, no. 4A, pp. A1133–A1138, Nov. 1965.

62 J. P. Perdew and A. Zunger, "Self-interaction correction to density-functional approximations for many-electron systems," *Phys. Rev. B*, vol. 23, no. 10, pp. 5048–5079, May 1981.

63 J. P. Perdew and Y. Wang, "Accurate and simple analytic representation of the electron-gas correlation energy," *Phys. Rev. B*, vol. 45, no. 23, pp. 13244–13249, Jun. 1992.

64 J. P. Perdew, K. Burke, and M. Ernzerhof, "Generalized Gradient Approximation Made Simple," *Phys. Rev. Lett.*, vol. 77, no. 18, pp. 3865–3868, Oct. 1996.

65 J. P. Perdew, A. Ruzsinszky, G. I. Csonka, O. A. Vydrov, G. E. Scuseria, L. A. Constantin, X. Zhou, and K. Burke, "Restoring the Density-Gradient Expansion for Exchange in Solids and Surfaces," *Phys. Rev. Lett.*, vol. 100, no. 13, p. 136406, Apr. 2008.

66 A. D. Becke, "A new mixing of Hartree–Fock and local density-functional theories," *J. Chem. Phys.*, vol. 98, no. 2, pp. 1372–1377, Jan. 1993.

67 S. L. Dudarev, G. A. Botton, S. Y. Savrasov, C. J. Humphreys, and A. P. Sutton, "Electron-energy-loss spectra and the structural stability of nickel oxide: An LSDA+U study," *Phys. Rev. B*, vol. 57, no. 3, pp. 1505–1509, Jan. 1998.

68 A. I. Liechtenstein, V. I. Anisimov, and J. Zaanen, "Density-functional theory and strong interactions: Orbital ordering in Mott-Hubbard insulators," *Phys. Rev. B*, vol. 52, no. 8, pp. R5467–R5470, Aug. 1995.

69 R. Clausius, *Die Mechanische Behandlung der Electricität*. Wiesbaden: Vieweg+Teubner Verlag, 1879.

70 R. Resta, "Theory of the electric polarization in crystals," *Ferroelectrics*, vol. 136, no. 1, pp. 51–55, Nov. 1992.

71 R. Resta, "Macroscopic polarization in crystalline dielectrics: the geometric phase approach," *Rev. Mod. Phys.*, vol. 66, no. 3, pp. 899–915, Jul. 1994.

72 T. Birol, N. A. Benedek, H. Das, A. L. Wysocki, A. T. Mulder, B. M. Abbett, E. H. Smith, S. Ghosh, and C. J. Fennie, "The Magnetoelectric Effect in Transition Metal Oxides: Insights and the Rational Design of New Materials from First Principles," Jul. 2012.

73 J. H. Lee, L. Fang, E. Vlahos, X. Ke, Y. W. Jung, L. F. Kourkoutis, J.-W. Kim, P. J. Ryan, T. Heeg, M. Roeckerath, V. Goian, M. Bernhagen, R. Uecker, P. C. Hammel, K. M. Rabe, S. Kamba, J. Schubert, J. W. Freeland, D. A. Muller, C. J. Fennie, P. Schiffer, V. Gopalan, E. Johnston-Halperin, and D. G. Schlom, "A strong ferroelectric ferromagnet created by means of spin–lattice coupling," *Nature*, vol. 466, 2010.

74 H. Chen and A. J. Millis, "Comparative study of exchange-correlation functionals for accurate predictions of structural and magnetic properties of multiferroic oxides," *Phys. Rev. B*, vol. 93, no. 20, pp. 1–7, 2016.

75 G. Giovannetti, S. Kumar, C. Ortix, M. Capone, and J. Van Den Brink, "Microscopic origin of large negative magnetoelectric coupling in $Sr_{1/2}Ba_{1/2}MnO_3$," *Phys. Rev. Lett.*, vol. 109, no. 10, pp. 1–5, 2012.

76 R. Nourafkan, G. Kotliar, and A.-M. S. Tremblay, "Electric polarization of $\mathbf{Sr_{0.5}Ba_{0.5}MnO_3}$ *Phys. Rev. B*, vol. 90, no. 22, p. 220405, 2014.

77 E. Bousquet and A. Cano, "Non-collinear magnetism in multiferroic perovskites," *J. Phys. Condens. Matter*, vol. 28, no. 12, p. 123001, Mar. 2016.

78 G. Kresse and J. Furthmüller, "Efficient iterative schemes for *ab initio* total-energy calculations using a plane-wave basis set," *Phys. Rev. B*, vol. 54, no. 16, pp. 11169–11186, Oct. 1996.

79 G. Kresse and D. Joubert, "From ultrasoft pseudopotentials to the projector augmented-wave method," *Phys. Rev. B*, vol. 59, no. 3, pp. 1758–1775, Jan. 1999.

80 E. Langenberg, L. Maurel, N. Marcano, R. Guzmán, P. Štrichovanec, T. Prokscha, C. Magén, P. A. Algarabel, and J. A. Pardo, "Controlling the Electrical and Magnetoelectric Properties of Epitaxially Strained $Sr_{1-x}Ba_xMnO_3$ Thin Films," *Adv. Mater. Interfaces*, vol. 4, no. 9, p. 1601040, May 2017.

81 A. Ohtomo and H. Y. Hwang, "A high-mobility electron gas at the $LaAlO_3/SrTiO_3$ heterointerface," *Nature*, vol. 427, no. 6973, pp. 423–426, Jan. 2004.

82 T. Ichinose, H. Naganuma, K. Mukaiyama, M. Oogane, and Y. Ando, "Preparation of monoclinic $0.9(BiFeO_3)$–$0.1(BiCoO_3)$ epitaxial films on orthorhombic $YAlO_3$ (100) substrates by r.f. magnetron sputtering," *J. Cryst. Growth*, vol. 409, pp. 18–22, Jan. 2015.

83 T. Takeda and S. Ōhara, "Magnetic Structure of the Cubic Perovskite Type $SrMnO_3$," *J. Phys. Soc. Japan*, vol. 37, no. 1, pp. 275–275, Jul. 1974.

84 R. J. Zeches, M. D. Rossell, J. X. Zhang, A. J. Hatt, Q. He, C.-H. Yang, A. Kumar, C. H. Wang, A. Melville, C. Adamo, G. Sheng, Y.-H. Chu, J. F. Ihlefeld, R. Erni, C. Ederer, V. Gopalan, L. Q. Chen, D. G. Schlom, N. A. Spaldin, L. W. Martin, and R. Ramesh, "A strain-driven morphotropic phase boundary in $BiFeO_3$.," *Science*, vol. 326, no. 5955, pp. 977–80, Nov. 2009.

85 L. Bellaiche and D. Vanderbilt, "Intrinsic Piezoelectric Response in Perovskite Alloys: PMN-PT versus PZT," *Phys. Rev. Lett.*, vol. 83, no. 7, pp. 1347–1350, Aug. 1999.

86 V. Goian, E. Langenberg, N. Marcano, V. Bovtun, L. Maurel, M. Kempa, T. Prokscha, J. Kroupa, P. A. Algarabel, J. A. Pardo, and S. Kamba, "Spin-phonon coupling in epitaxial $Sr_{0.6}Ba_{0.4}MnO_3$ thin films," *Phys. Rev. B*, vol. 95, no. 7, p. 75126, Feb. 2017.